电 化 学
J. Electrochem. 2022, 28(9), 2214004 (1 of 30)

[Review] DOI: 10.13208/j.electrochem.2214004 Http://electrochem.xmu.edu.cn

Perovskite-Type Water Oxidation Electrocatalysts

Xiao Liang, Ke-Xin Zhang, Yu-Cheng Shen, Ke Sun, Lei Shi, Hui Chen,
Ke-Yan Zheng*, Xiao-Xin Zou*

(*State Key Laboratory of Inorganic Synthesis and Preparative Chemistry, College of Chemistry, Jilin University, Changchun 130012, P. R. China*)

Abstract: The development of energy conversion/storage technologies can achieve the reliable and stable renewable energy supply, and bring us a sustainable future. As the core half-reaction of many energy-related systems, water oxidation is the bottleneck due to its sluggish kinetics of the four-concerted proton-electron transfer (CPET) process. This necessitates the exploitation of low cost, highly active and stable water oxidation electrocatalysts. Perovskite-type oxides possess diverse crystal structures, flexible compositions and unique electronic properties, enabling them ideal material platform for the optimization of catalytic performance. In this review, we provide a comprehensive summary for the crystal structures, electronic structures and synthetic methods of perovskite-type oxides in their application background of water oxidation electrocatalysis. Then, we summarize the recent research advances of perovskite-type water oxidation electrocatalysts in alkaline and acidic media, and highlight the significance of their structure-activity relationship and activation/deactivation mechanism. Finally, challenges and the corresponding solutions for the perovskite-type electrocatalysts are highlighted, which is expected to open the opportunities to their practical applications.

Key words: perovskite; water oxidation; electrocatalysis; water splitting; hydrogen energy

1 Introduction

Excessive exploitation and use of fossil fuels have exacerbated environmental pollution and climate change, thereby threatening human survival and development. The utmost urgency is to adjust the current energy structure and to reduce carbon emissions by effectively utilizing renewable energy sources (*e.g.*, solar and wind)[1-4]. These initiatives will provide considerable economic and ecological values to society. However, renewable energy sources are usually intermittent and volatile, making them difficult to directly integrate into the power grid[5-7]. Sustainable energy supply requires efficient energy storage and conversion technologies. Water oxidation, also known as oxygen evolution reaction (OER), acts as the anode half-reaction in several energy conversion/storage systems, such as water splitting, carbon dioxide reduction, nitrogen reduction and metal-air batteries. More importantly, in these energy systems, water oxidation occupies the core position (Figure 1) and determines their energy transformation efficiency. Unfortunately, water oxidation involves four proton/electron coupling steps. Its sluggish reaction kinetics severely limits the efficiency of energy devices, and even restricts the industrialized application of the corresponding technologies. Therefore, great efforts have been devoted to the exploitation of high-performance water oxidation electrocatalysts to

Cite as: Liang X, Zhang K X, Shen Y C, Sun K, Shi L, Chen H, Zheng K Y, Zou X X. Perovskite-type water oxidation electrocatalysts. *J. Electrochem.*, 2022, 28(9): 2214004.

Received: 2022-06-16, Revised: 2022-07-24. *Corresponding author, Zheng Ke-Yan, Tel: (86)13504331305, zhky@jlu.edu.cn; Zou Xiao-Xin, Tel: (86-431)85168221, E-mail: xxzou@jlu.edu.cn.

promote the development of energy conversion/storage devices[8,9]. In particular, perovskite-type oxide electrocatalysts with great structural and compositional flexibility have attracted much attention[10].

Perovskite has experienced several "boom" periods for various applications since its discovery (Figure 2). The publication of perovskite goes back to 1839, when Prussian mineralogist Gustav Rose first discovered a mineral composed of calcium titanate ($CaTiO_3$) from chlorite-rich skarn. The new mineral was named after the Russian mineralogist L. A. Perovski[11]. Later, researchers have discovered some natural minerals (*e.g.*, $FeTiO_3$ and $MgSiO_3$) and synthesized various oxides (e.g., manmade $CaTiO_3$ and $NaNbO_3$), who share the similar or derived crystal structures to perovskite[12,13]. These minerals and oxides are then grouped into a perovskite family, and nowadays the term of inorganic perovskite represents a type of material with the general formula ABX_3 (A = alkaline/alkaline-earth/rare-earth elements, B = transition metal/rare-earth elements, X = oxygen/halogen elements). The first case of perovskite as a material is $CaTiO_3$ pigment, which was applied for an industrial patent by V. M. Goldschmidt in 1922[13]. In the 1940s, several research teams around the world almost simultaneously discovered the high dielectric constant (two orders of magnitude higher than other dielectric materials) of $CaTiO_3$ ferroelectrics, and perovskite stepped into its first boom for the electronic age[12, 14]. The second perovskite boom arrived in 1986, when G. Bednorz and A. Müller synthesized distorted $La_{1-x}Ba_x$-CuO_4 with the high-temperature superconductivity[15]. This discovery detonated the upsurge of superconductivity research and granted them the Nobel Prize for Physics in 1986. The magnetic perovskite became a research hotspot until 1990s, even though the ferromagnetism and magnetoresistance of $Ln_{1-x}A_xMnO_3$ (Ln = lanthanide, A = alkaline earth cation) were first discovered by G. H. Jonker and J. H. Van Santen in 1950[16]. After entering the 21st century, the applications in energy conversion/storage of perovskite are further discovered. The Miyasaka group reported $CH_3NH_3PbI_3$ perovskite with the high photochemical activity in 2006, and started a perovskite period for solar cell[17]. In the past decade, the electrocatalytic applications of perovskite thrive. Even though the $LaCoO_3$ was the first reported oxygen electrocatalyst in 1970, the prospects of perovskite-type electrocatalysts are actually identified since the advents of $Ba_{0.5}Sr_{0.5}Co_{0.8}Fe_{0.2}O_{3-\delta}$ (The Shao-Horn group, 2011) and $SrIrO_3$ (The Jaramillo group, 2016). Undoubtedly, we are currently in the golden period of a new "perovskite boom"[18-20].

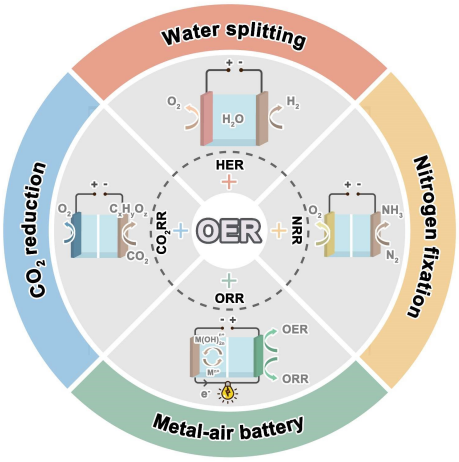

Figure 1 Schematic illustration showing the core position of water oxidation in multiple energy systems. (color on line)

The various applications of perovskite-type materials can be attributed to their unique structural diversity, component flexibility and tunable electronic structure. There exist the polymorphs with different crystal phases (*e.g.*, cubic, orthorhombic or hexagonal) for a perovskite-type oxide. And a number of perovskite-derived structures have emerged, including double, triple, quadruple and layered perovskite, etc. These diverse crystal structures create a vast space for material design[21-23]. It has been reported that there are 49 possible A-site and 68 possible B-site elements in perovskite-type oxide, which accounts for ~90% of the elements on the periodic table. And the combination of cations A and B results in 3332 different perovskite-type oxides[24]. The wide element coverage facilitates the regulation of electronic properties of perovskite-type oxide. Moreover, A- and B-site cations in perovskite-type oxides can be sub-

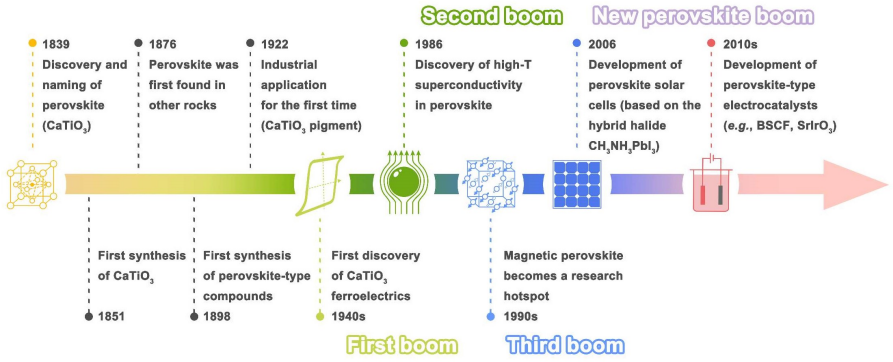

Figure 2 History timeline infographic of perovskite. (color on line)

stituted by multiple elements with different contents (*e.g.*, $A_xA'_{1-x}BX_3$ and $AB_yB'_{1-y}X_3$), which leads to the material library of perovskite-type oxides to be almost boundless. And the exploration of the regularity for properties can be realized by the adjustable continuously composition. This is why the perovskite-type oxide has long been regarded as a research platform for water oxidation electrocatalyst, benefiting from the controllable modulation of various electronic properties (*e.g.*, adsorption strength of intermediates, energy band structure and orbital hybridization) [10]. Inspired by these advantages, researchers have developed numerous perovskite-type water oxidation electrocatalysts that possess high activity, good stability and/or low cost.

Herein, we review the recent advances of perovskite-type electrocatalysts for water oxidation. We introduce the general features of crystal and electronic structures of perovskite oxides, and summarize the representative synthetic strategies developed to obtain perovskite oxides. We then discuss the research progress of perovskite-type water oxidation electrocatalysts in acidic and alkaline media, with an emphasis on structure-activity relationship for perovskite-type electrocatalysts. Finally, we summarize the remaining challenges and outlook the further opportunities of perovskite-type electrocatalysts for water oxidation.

2 Basics of Perovskite

2.1 Crystal Structures of Perovskite

The ideal perovskite-type structure, also known as aristotype, is a cubic close-packed structure with the space group *Pm-3m*. In such a cubic unit cell (Figure 3a), cations B are generally considered as the cell origin, with the Wyckoff positions as 1*a* (0, 0, 0), and occupy the eight corners of the unit cell. They are surrounded by 6 anions X, which locate at the midpoint of cell edges (3*d* (1/2, 0, 0)), forming the BX_6 octahedra. Cation A lies at the center of the unit cell (1*b* (1/2, 1/2, 1/2)) with a coordination number of 12. These build up a three-dimensional framework of corner-shared BX_6 octahedra, and the crystal struc-

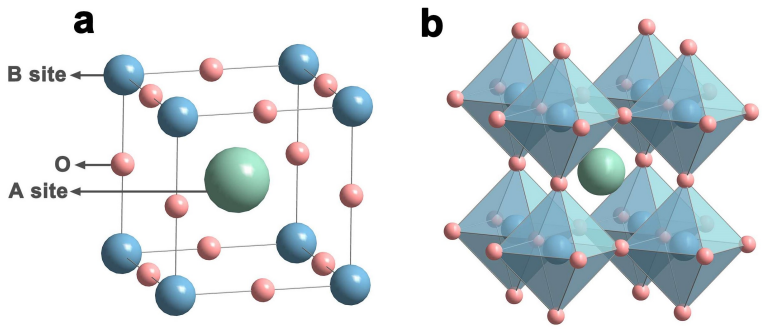

Figure 3 (a) Unit cell of ideal perovskite-type structure. (b) Octahedra framework of perovskite-type structure. (color on line)

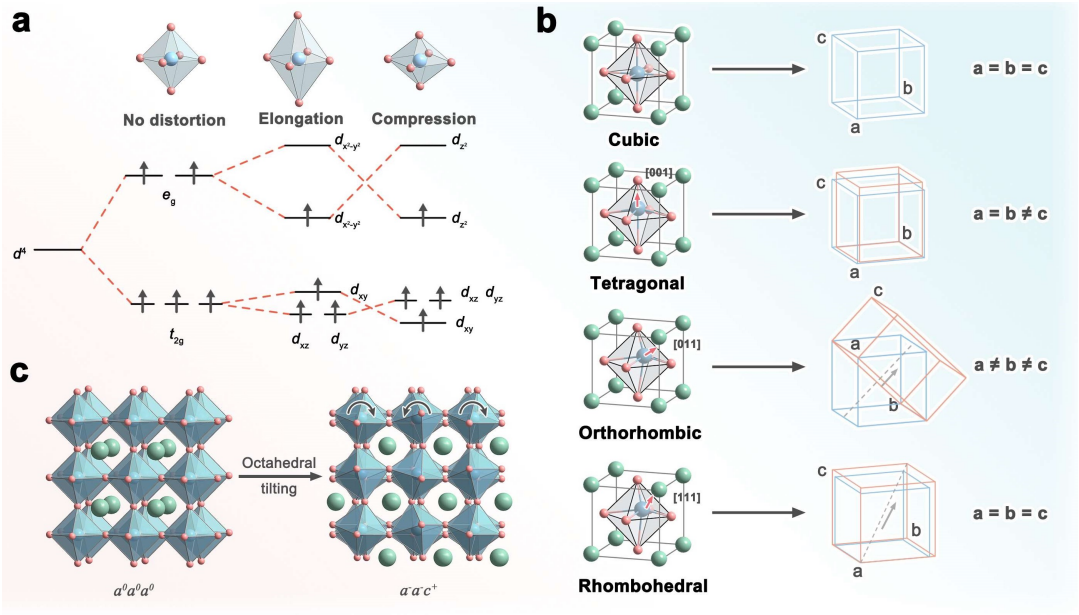

Figure 4 Three distortion mechanisms of perovskite-type structure, including (a) octahedral distortion, (b) B-cation displacement, (c) octahedral tilting. (color on line)

ture of perovskite can also be presented in another way as shown in Figure 3b, which is conducive to the discussion of structural variation and electronic property.

The perovskite with an idealized cubic structure (*e.g.*, $SrTiO_3$) is rare. Even the firstly discovered perovskite $CaTiO_3$, it actually exhibits an orthorhombic structure. In term of the majority of perovskites, their symmetries of crystal structures tend to be suppressed to evolve the derivative structures, arising from the mechanisms including octahedral distortion, B-cation displacement, and octahedral tilting[25, 26]. These structural variations often induce a phase transition, which can further significantly affect the electronic properties of perovskite.

Octahedral distortion in perovskite-type structure originates from the Jahn-Teller (JT) effect. JT distortion occurs, when a nonlinear molecule exhibits both symmetrical atomic configuration and degenerated electronic ground state. In the case of BX_6 octahedra in perovskite, its energy levels of d electrons in the cation B split into two groups of orbitals: e_g orbitals *i.e.*, d_{z^2} and $d_{x^2+y^2}$ at upper energy level, and t_{2g} orbitals (*i.e.*, d_{xy}, d_{yz} and d_{xz}) at lower energy level. With respect to some perovskite-type materials, their cations B has the odd number of d-electron in e_g orbital, such as $Mn^{3+}(t_{2g}^3e_g^1)$ and $Cu^{2+}(t_{2g}^6e_g^3)$, exhibiting the degenerated electronic ground state. These lead to the structurally instability. In order to remove the degeneracy, the corresponding perovskite-type structures have to lower their overall energy by undergoing a geometrical distortion. There are two types of BX_6 octahedral distortion: elongated and compressed (Figure 4a). These shapes of octahedra arise from the further splitting of e_g, and t_{2g} orbitals, and are dominated by the splitting of the e_g orbitals. It is difficult to predict qualitatively the favored octahedral distortion, but BX_6 octahedral elongation (*e.g.*, $LaMnO_3$) accounts for the majority of reported perovskite-type materials, leading to the tetragonal or orthorhombic phase[27]. In some extreme cases, the JT distortion can result in the square pyramidal (*e.g.*, $YBa_2Cu_3O_7$)[28], and even square planar (*e.g.*, $CaCu_3Fe_4O_{12}$) geometries[29].

The origin of B-cation displacement is the too small effective size or the electronic instability of cation B. The former occurs when the B-X bond length is less than the half of effective size of anion X. And the latter is due to the second order JT effect. A well-known example is $BaTiO_3$, whose Ti^{4+} exhibits a nondegenerate electronic ground state and a fairly

low-ly ing excited state. An off-center displacement of Ti^{4+} in TiO_6 octahedra is able to mix the ground and excited states, and thus to reduce the ground-state energy. It is noteworthy that JT distortion and B-cation displacement are sensitive to temperature and pressure. Under different conditions, the cation B displaces along the symmetry axes of the BX_6 octahedra with varying degree, giving rise to a phase transition to the perovskite-type structure with lower symmetry (Figure 4b). In the case of $BaTiO_3$, when the temperature increases from 183 to 393 K, the Ti^{4+} displaces sequentially along [111], [011], [001] crystallographic directions, and then returns to center. These displacements result in the rhombohedral-orthorhombic-tetragonal-cubic phase transition.

Octahedral tilting is the most common phase-transition mechanism in perovskite-type structure, which attributes to the mismatch of A-X and B-X bond lengths. In some perovskites, the effective sizes of their cations A are too small to be coordinated with the anions X. The corner-shared BX_6 octahedrons are analogous to the flexible hinge, allowing their tilting and rotation to reduce the space of A-site cavity. Then, the connectivity between the cation A and anion X will be maintained, enhancing the stability of perovskite-type structure. And the tilting of one BX_6 octahedron will trigger a chain tilting of others in the framework, which results in the phase transition. Octahedral tilting has a standard description known as Glazer notation[30]. It defines the cubic aristotype as the start, and three orthogonal crystallographic axes as the tilting axes. The magnitudes of rotations along three tilting axes can be specified by letters *a*, *b*, and *c*, and the same letter can be employed when the tilting amplitude is same. The superscripts +, - and 0 represent the same, opposite and no tilt of two linked layers along the corresponding axis, respectively. For instance, the cubic $SrTiO_3$ without octahedral tilting can be denoted as $a^0a^0a^0$. The orthorhombic distortion of $CaTiO_3$ (*Pnma*, #62) can be described as $a^-a^-c^+$ (Figure 4c). Similar to the other two distortion mechanisms, octahedral tilting is sensitive to the external condition (*e.g.*, temperature, pressure and strain), which is potential to derive a variety of crystal phase such as orthorhombic, tetragonal, rhombohedral, monoclinic and triclinic.

In fact, these three distortion mechanisms are not mutually exclusive, but often simultaneously occur and synergically impact with each other during the formation of perovskite-type structure. It is the corresponding structural variation that enlarges the crystal system of perovskite family, which includes cubic, tetragonal, orthorhombic, hexagonal, monoclinic and triclinic perovskite-type structures. In such a large family, a descriptor, which can quantitatively estimate the structural distortion, is required. For this purpose, V. M. Goldschmidt proposed a descriptor called tolerance factor (t)[31], which can be calculated by Equation (1):

$$t = \frac{(r_A + r_X)}{\sqrt{2}\,(r_B + r_X)} \tag{1}$$

where r_A, r_B, and r_X represent the effective ionic radii of the cation A, cation B and anion X. For the cubic perovskite-type oxides, their t is close to unity within a small range of 0.9 ~ 1(*e.g.*, $SrTiO_3$). For the range of 0.71 ~ 0.9, the crystal structure is orthorhombic or rhombohedral. When t ranges from 1 to 1.13, the phase transition into hexagonal or tetragonal structure will occur. In addition, this parameter is also capable of describing the stability of perovskite-type structures. When t is within the range of 0.71 ~ 1.13, the corresponding perovskite-type structure can be formed. Otherwise, it will be further dis torted and even collapsed.

Besides the simple perovskite discussed above, there are several subclasses of perovskite, including double, triple, quadruple and layered perovskites. They possess more complex structures, which contain more than one layer of AX_{12} and/or BX_6 polyhedral slabs in a unit cell. These perovskite derivatives further stretch the structural and compositional boundaries of perovskite family, and endow perovskite-type structure with some unique electronic properties.

The cation A (or B) in simple perovskite can be partially replaced by the other cation A′ (or B′). The cation A′ (or B′) randomly occupies the A (or B) sites

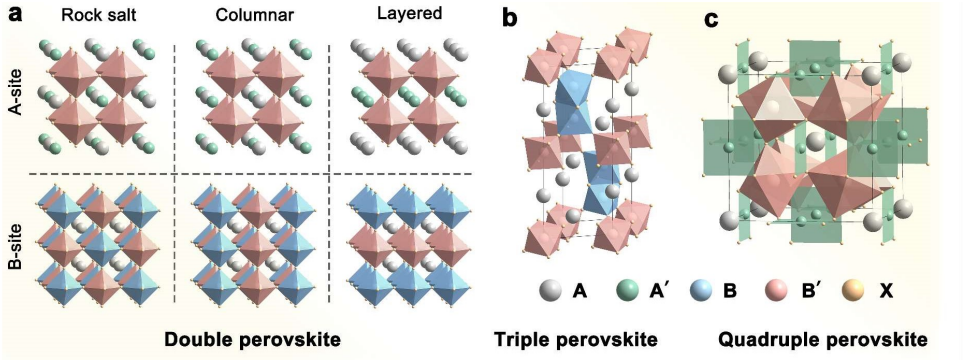

Figure 5 Crystal structures of (a) double perovskites with different cation ordering schemes, (b) triple perovskite, (c) quadruple perovskite. (color on line)

in pristine perovskite, resulting in the formation of doped perovskite $A_{1-x}A'_xBX_3$ (or $AB_{1-y}B'_yX_3$). Once the molar ratio of A′ (or B′) reaches to 50% and the foreign cations possess significantly different radii and/or valence states from the original cation, the cations A and A′ (or B and B′) are possibly arranged in an order manner. The unit cell of this resulting crystal structure contains double BX_6 octahedrons along each axis against the pristine unit cell of simple perovskite (Figure 5a). Therefore, the corresponding crystal structure is named by double perovskite, with a formula of $AA'B_2X_6$ (or $A_2BB'X_6$)[21]. In double perovskite, the ordered distribution of A and A′ (or B and B′) can be divided into three types, including rock-salt ordering, columnar ordering and layered ordering (Figure 5a). Among these arrangements, layered ordering and rock-salt ordering are most common for cations A and B, respectively[32].

Double perovskite gives more possibilities to the adjustments of composition and structure for perovskite-type materials. In term of composition, it accommodates more components compared to simple perovskite. In addition, double perovskite can adapt the cation B with high valence (*e.g.*, BVI and BVII), which is impossible to be accommodated in simple perovskite. Moreover, the alternation of BX_6 octahedra by $B'X_6$ octahedrons will significantly vary the geometric coordination environment of perovskite-

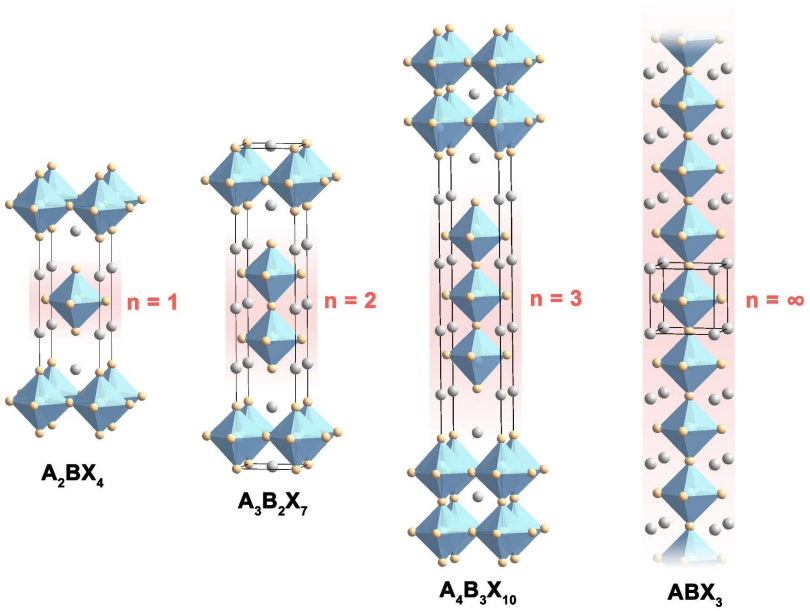

Figure 6 Crystal structures of Ruddlesden-Popper perovskites, $A_{n+1}B_nX_{3n+1}$ (n = 1, 2, 3, and ∞). (color on line)

type structure and tend to drive a positive bimetallic synergy between cations B and B′.

The further compositional expansion of perovskite does not stop with double perovskite, rather develops multiple novel perovskite derivatives, such as triple perovskite (*e.g.*, $Ba_3TiIr_2O_9$, Figure 5b)[22] and quadruple perovskite (*e.g.*, $CaCu_3Fe_4O_{12}$, Figure 5c)[29]. In particular, quadruple perovskite has caught the attention of researchers, attributing to its interesting geometric coordination environment. In quadruple perovskite, pristine cation A is 20-fold coordinated by O_2^-, and foreign cation A′ occupies 3/4 of the original A site with a square-planar coordination. It is worth noting that A' site can accommodate transition metal (*e.g.*, Cu and Mn), which is totally different from simple perovskite and double perovskite. The unique crystal structure of quadruple perovskite not only widens the selection of elements, but also proves to enhance the structural stability of perovskite-type material.

Layered perovskites contain Ruddleson-Popper (R-P), Dion-Jacobson (D-J) and Aurivillius phases. The latter two have almost never been reported in catalysis. Therefore, we focus on the crystal structure of R-P phase. In 1957, S.N. Ruddlesden and P. Popper first synthesized a series of compounds (*e.g.*, Sr_2TiO_4, Ca_2MnO_4 and $SrLaAlO_4$) with a novel crystal structure[33]. Later, these compounds are known as R-P perovskite, with a general formula of $A_{n+1}B_nX_{3n+1}$ (n = 1, 2, 3, ⋯). In R-P perovskite (Figure 6), the perovskite-type layers (ABX_3) and rock-salt-type layers (AX) are alternately and periodically stacked along c-axis direction. Due to this layer structure characteristics, the formula of R-P perovskite can also be written as $AX(ABX_3)_n$. And n stands for the number of BX_6 octahedrons along c-axis in ABX_3 layer, which is sandwiched between two AX layers. It can be observed that the dimensionality of R-P perovskite has a positive correlation with the value of n. When n is next to infinity ($n \rightarrow \infty$), the crystal structure of R-P perovskite will be transformed from two-dimensional to three-dimensional arrangement (2D→3D), resulting in a well-known simple perovskite- type structure. Besides, the preparation of R-P perovskite will be more difficult as the value of n increasing. It has been reported that once $n > 3$, R-P perovskite will become thermodynamically unstable. Thus, the synthesis and characterization of R-P perovskite are concentrated on A_2BX_4 (n = 1), $A_3B_2X_7$ (n = 2), $A_4B_3X_{10}$ (n = 3) until now[23].

The layered structure introduces some benefits to the further modifications for R-P perovskite. On the one hand, the interlayer cations between ABO_3 layer and AO layer are likely to be exchanged with other cations, facilitating the intercalation modification. On the other hand, the R-P structure is promising to be exfoliated into ultrathin 2D nanomaterials, using the synthetic methods such as mechanical force-, ion intercalation-, or ion exchange-assisted liquid exfoliations. The acquired 2D nanomaterials are feasible to expose more active sites and present unique coordination environment on the surface.

Researches in the phase transition and the complex structure of perovskite are highly attractive for exploiting functional materials. In such a large perovskite family, the diverse crystal structures give rise to a wide range of unique electronic structures and thus lead to multiple applications. In the field of electrocatalysis, tuning the crystal structure and composition of perovskite-type catalyst will significantly affects its electronic properties, such as adsorption strength and energy band structure. This provides an opportunity to investigate structure-catalytic performance with perovskite as the model materials, and to exploit next-generation electrocatalysts with higher efficacy and/or new catalytic ability.

2.2 Electronic Structure of Perovskite

From the perspective of molecular orbital theory, electronic structure refers to the linear combination of atomic orbitals. With the application of solid state physics in chemistry, electronic structure is also inseparable from the band theory, which embodies the relationship between electronic properties and physiochemical properties of crystal. Each orbital type (*s*/*p*/*d*/*f*) of each atom contributes to the electronic band structure, and small changes in some key or-

bitals can have significant effects on the bands[34]. In most perovskites, the *d* orbitals of the B-site transition metal and *p* orbitals of the oxygen contribute mostly to the conduction band and valence band near the Fermi level. This local band structure plays a critical role in many catalytic processes. On the contrary, the band of the A-site ion has a contribution to the band structure far away from the Fermi level[25].

The simplest type of perovskite oxide, *e.g.*, insulating cubic $SrTiO_3$, is used to describe the general electronic structure (Figure 7a). For the group of bands at the top of the valence band of the crystal, it is mainly derived from the 2*p* orbitals of the three oxygens in the unit cell. The Fermi level sits on top of these bands. For the set of bands forming the bottom of the conduction band, it comes from the 3*d* orbitals of Ti with octahedral coordination. Due to structural symmetry, the band of the double degenerate eg orbital is higher than that of the triple degenerate t_{2g}. There is a band gap between the bottom of the conduction band and the top of the valence band. In addition, although other high-energy bands of orbitals exist (*e.g.*, Ti 4*s* and 4*p* orbitals), their effect on electron properties is not as important as the bands described above. Furthermore, the density of states (DOS) derived from band structure, i.e., as a function of energy across the bands, gives the distribution of energy levels in different bands (Figure 7b). This is very helpful in simplifying the analysis of the effect of the electronic structure on the actual related properties. In perovskite, it has been established that 3*d* bands and 2*p* bands largely determine the catalytic properties. So naturally, the focus of research falls on how the 3*d* bands, 2*p* bands and even the interaction between them affect the reactivity of the catalyst.

For water oxidation, the activity of perovskite catalyst is determined by the adsorption of oxygen-containing intermediates on its surface, which is essentially metal-oxygen bonding. From the perspective of coordination chemistry, the metal *d* and oxygen 2*p* orbitals in the octahedral coordination BO_6 of the bulk of perovskite are hybridized to form high spatial overlap σ orbitals and low spatial overlap π orbitals[10].

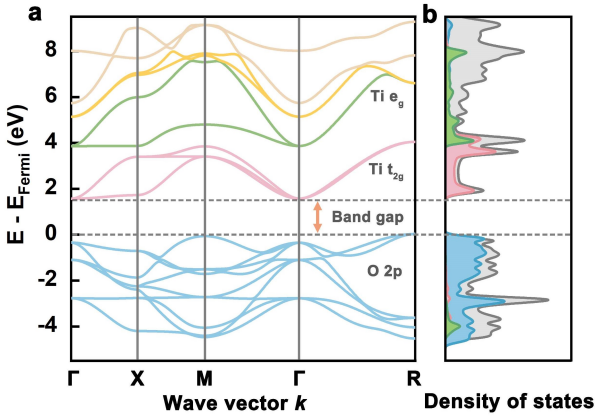

Figure 7 (a) The approximate band structure of cubic $SrTiO_3$. (b) Density of states corresponding to (a), where the contributions of Ti *eg*, Ti t_{2g} and O 2*p* to total DOS are represented in green, pink and blue, respectively. (color on line)

The σ and π antibonding orbitals are composed of the e_g and t_{2g} orbitals, respectively. Since all catalytic reactions occur on the surface, the surface unsaturated coordination of BO_5 in perovskite, as the active site, can more accurately describe the metal-oxygen bonding involved in the reaction. In contrast to the bulk, the symmetry breaking further splits the e_g and t_{2g} orbitals into different energy levels (Figure 8a). This eg-like state has a stronger overlap with corresponding orbital of oxygen than t_{2g} state due to its good vertical orientation with adsorption intermediates. Therefore, from the maximum overlap population principle, e_g occupation describes the bonding strength of the adsorbed intermediate to the surface. And because e_g orbital participates in the formation of σ-antibonding orbital, the less e_g filling corresponds to the stronger bonding strength.

The study by Shao-Horn's group pointed out that the e_g filling of perovskite catalysts with the best OER activity was about 1.2[19]. This can be achieved by taking full advantage of the flexibility of the composition of perovskite, that is, by substituting A site and B site to change the oxidation state of the transition metal at B site, thus changing the e_g filling. On the other hand, strain can be used to break the symmetry of the ideal octahedron of BO_6, so that the electron occupation of *d* orbital has an asymmetry to modulate e_g filling[35].

Although e_g filling has been demonstrated, perovskites with the same e_g filling (*e.g.*, $LaMnO_3$, $LaCoO_3$, $LaNiO_3$) have significantly different catalytic activities, which confuses the use of this description[36]. On the other hand, due to the complex spin states of some Co-based perovskites, it is difficult to accurately measure e_g filling, which limits its wide application. Therefore, Shao-Horn's group proposed the position of the O *p*-band center relative to the Fermi level as an effective electronic structure descriptor[37, 38]. They have shown that this descriptor determines the degrees of oxygen migration and oxygen vacancy formation, which regulates the adsorption of intermediates and thus affects OER activity. When the center of O *p*-band moves to the Fermi level, the OER activity increases, but when the center of O *p*-band is too close to the Fermi level, the stability decreases, which may be due to the structural instability caused by too fast oxygen exchange. Furthermore, the effect of O *p*-band center on OER can be qualitatively explained by a simple rigid band model (Figure 8b). In this model, adding O to the system corresponds to moving electrons from the Fermi level to the O *p*-band (while removal of oxygen corresponds to moving electrons in the opposite direction). Specifically, when oxygen is removed (added), the 2*p*-state of oxygen decreases (increases) and the Fermi energy level rises (falls) relative to the transition metal 3*d*-state. Therefore, the change in the number of interchanged electrons between the Fermi level and the O *p*-band affects the reaction energy.

For late transition metal water oxidation catalysts, p-band center descriptor is not applicable, because most of them are semiconductor or insulator oxides, and their Fermi levels are in the band gap region, making the exact position difficult to be determined. To deal with this problem, Shao-Horn's group proposed a charge transfer energy descriptor and confirmed that this descriptor is universal to metallic, semiconducting and insulating oxides[39]. The charge transfer

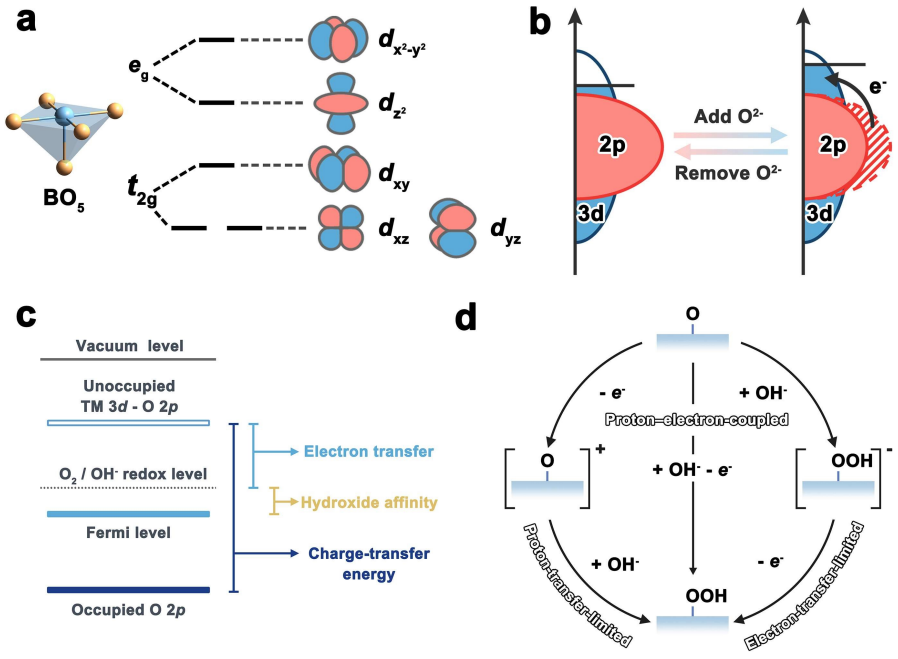

Figure 8 (a) The split energy levels and the corresponding shapes of the *d* orbitals in BO_5 configuration. (b) Schematic diagram of the electron structure to illustrate the role of O *p*-band in regulating OER energies, where the blue and red regions represent occupied metal 3*d*-states and O 2*p*-states respectively. (c) Schematic diagram of the energy levels used to calculate electron transfer, hydroxide affinity, and charge transfer energy of the oxides. (d) Three cases of proton and electron transfers in the rate-limiting step from the O intermediate to the OOH intermediate. It represents the coupled or decoupled proton electrons under electron affinity and hydroxide affinity. (color on line)

energy is the relative position of transition metal 3*d* and O 2*p* valence electronic states, that is, the covalence of the M-O bond, which can be obtained by X-ray emission spectroscopy (XES) and X-ray absorption spectroscopy (XAS). It can regulate the electron delocalization and redox couple of oxides to impact the kinetic and mechanism of water oxidation.

From absolute energy scale of the partial density of states (PDOS)[40], the electronic structure of charge transfer energy is further analyzed (Figure 8c). The unoccupied transition metal (TM) 3*d*-band position mainly affects the charge transfer energy because many perovskite oxides possess similar O-2*p* energy levels. This explains why many studies regard *d*-electron number and metal oxidation state as descriptors of OER activity, because atomic number and oxidation state have a strong influence on band position of TM 3*d*[41]. More importantly, band positions determined by charge transfer energy can decouple electron and chemical interactions at the reaction interface by influencing electron transfer kinetics and hydroxide affinity. Firstly, the electron transfer kinetics can be reflected by the electron affinity of the oxide with respect to the electrolyte, the Schottky barrier[42] of the electron transfer step, which is defined as the energy difference between the unoccupied TM 3*d*-O 2*p* band and the redox potential of the electrolyte. High charge transfer energy corresponds to high Schottky barrier and poor material conductivity[43]. In addition, hydroxyl affinity is related to the position of Fermi energy level relative to redox potential, and largely determines the acid-base chemistry of oxides in electrolytes[44]. When the Fermi level of the oxide is lower than the OER potential energy, the oxide surface is negatively charged in equilibrium with the electrolyte, and the negative charge may come from the adsorption of hydroxide ions in the solution. Reducing the charge transfer gap between semiconductor oxides increases electron to surface mobility and reduces the need to adsorb hydroxide ions at the electrolyte interface to compensate for charge[45], resulting in more efficient electron screening at the surface. Finally, the competition between electron and hydroxide affinity may change the traditional OER four-concerted proton-electron transfer (CPET) mechanism (Figure 8d). With the gradual decrease of charge transfer energy, the reaction mechanism changes from electron-transfer-limited to proton-electron-coupled and then to proton-transfer-limited.

The above studies describe the effect of the electronic structure of perovskite on water oxidation through some simple models, and emphasize that this simple form contains profound physical and chemical principles. The electronic structure of the perovskite family is varied due to its flexible composition and structural tunability. This means that it is difficult to explain all catalytic phenomena with a single description of the electronic structure. But no matter how complex, the essence of electronic structure is firmly linked to catalysis. In the future, combined with more advanced computational and experimental techniques, more in-depth studies of electronic structure will provide a wide range of opportunities for understanding catalytic processes and screening highly active catalysts.

2.3 Synthetic Methods of Perovskite-Type Oxides

2.3.1 Solid-State Method

Traditionally, perovskite has been synthesized by the solid-state method. In the solid-state method, several metal oxides are mixed in a stoichiometric ratio and then calcined in air to obtain perovskite oxide powder. In the synthesis process, the raw materials usually need to be calcined at high temperature and/or high pressure for a long time. For example, Kumar et al. prepared $LaCo_{1-x}Ni_xO_3$ perovskite by traditional solid-state method[46]. Stoichiometric amounts of La_2O_3, CO_2O_3 and NiO were thoroughly mixed, ground, and then calcined in air at 900 °C and further at 1200 °C for certain time. Solid-state method can also be used for synthesizing perovskites with different structures and components, such as Ba_2MIrO_6 (M = La, Ce, Pr, Nd, Tb and Y), $BaCo_{0.9-x}Fe_xSn_{0.1}O_{3-\delta}$ (x = 0.2, 0.3, 0.4), and $Sr_{1-x}Nb_{0.1}Co_{0.7}Fe_{0.2}O_{3-\delta}$ (x = 0, 0.02, 0.05, 0.1)[47-49]. The solid-state method is easy to operate, and the synthesized samples have high crys-

tallinity and less defects. Meanwhile, some metastable crystal phases of perovskite can only be synthesized by solid-state method at present. Taking Ruddlesden-Popper iridate oxides ($Sr_{n+1}Ir_nO_{3n+1}$) as an example, high pressure and/or high temperature conditions are required to achieve this unique layered structure. However, this method often leads to large particle size and small specific surface area, which may lead to poor electrocatalytic performance. In addition, if the metal oxide reactants are mixed incompletely, there may be impurities in the products that affect catalytic performance of perovskite[50, 51].

2.3.2 Wet Chemistry-Assisted Solid-State Method

The use of a liquid medium in wet chemistry ensures more uniform precursors, which helps reduce the temperature of subsequent heat treatments, thereby inhibiting grain growth. In addition, some wet chemical methods (such as sol-gel, electrospinning, etc.) can introduce special chelating agents to affect the growth process of crystal phase in the calcination process, and realize controllable crystal phases, crystal planes, defects and other structural properties[52]. For example, Li et al. proposed a salt-templated strategy for fabrication of atomically thin perovskite oxide of $LaMnO_3$ and realized the synthesis of three different crystal phases $LaMnO_3$ (orthorhombic, tetragonal, and hexagonal) by controlling the annealing time[53]. Commonly used wet chemical-assist methods can be divided into the following categories.

In co-precipitation-assisted process, the metal precursor is dissolved in water to form an aqueous solution. Then co-precipitators (such as OH^-, CO_3^{2-}, etc.) are added to form insoluble hydroxides, hydration oxides or salts are precipitated from the solution. After cleaning the solvent and ions in the multi-component precipitated precursors, the precursors are calcined in air at a certain temperature to obtain perovskite powder. The co-precipitation method overcomes the disadvantage of inhomogeneous mixing in solid-state method and can accelerate the solid-solid reaction during heat treatment. Due to the decrease in calcination temperature, the particle size of perovskite prepared by this method changes from micronmeter to nanometer, which increases the specific surface area and improves the catalytic activity. Jin et al. synthesized urchin-like $La_{0.8}Sr_{0.2}MnO_3$ perovskite oxide with a high specific surface area by co-precipitation method using urea as a precipitator[54].

In sol-gel method-assisted process, the metal salt is dissolved in water or other solvents, and organic ligands (such as citric acid, ethylene glycol, etc.) are added to form complexes with metal ions. Then, the complex solution forms sol by controlling the temperature, pH and other conditions. Eventually, it polymerizes to form a gel. After drying, the perovskite oxide is obtained by calcination of the dried gel at a certain temperature. For example, Yu et al. synthesized $La_{0.4}Sr_{0.6}Co_{0.7}Fe_{0.2}Nb_{0.1}O_{3-\delta}$ by sol-gel method and solid-state method, respectively[55]. They found that the catalysts synthesized by sol-gel method had better catalytic activity. This is mainly due to the larger specific surface area, variation in the surface oxidation states of the Co cation, and high content of the highly oxidative oxygen species O_2^{2-}/O^-.

Electrospinning is usually used to prepare perovskite oxide nanofibers. In this method, a solution of the precursor (polymer and metal salt) is added to the syringe, and under the action of a high voltage electrostatic field, the polymer carries metal salt to form microjet deposition on the substrate. The organic matter in spinning is removed by sintering and the ideal perovskite nanofibers are obtained. Wang et al. synthesized $La_{0.8}Sr_{0.2}Co_{0.2}Fe_{0.8}O_{3-\delta}$ perovskite oxide by electrospinning and controlled the morphology of $La_{0.8}Sr_{0.2}Co_{0.2}Fe_{0.8}O_{3-\delta}$ (nanofibers, nanorods and nanoparticles) by adjusting the weight percentage of nitrate in the precursor solution[56]. Compared with nanorods and nanoparticles, one-dimensional nanofibers not only increase the specific surface area, but also enhance the efficient transport pathways of electrons and ions, and improve the catalytic performance.

2.3.3 Hydrothermal/Solvothermal Method

Different from the above two methods, hydrothermal/solvothermal can achieve one-step synthesis of perovskite at low temperature (usually below 300 °C) without subsequent solid-state reaction. Hydrother

mal/solvothermal method refers to the method of preparing materials by dissolving and recrystallizing powders in a sealed pressure vessel under solvent conditions. Compared with other preparation methods, the perovskite powders prepared by hydrothermal/solvothermal method often have the characteristics of small particle size and uniform distribution. The most classical reaction is the hydrothermal synthesis of barium titanate perovskite. Flaschen et al. described a direct solution route to $BaTiO_3$, reporting that a reaction temperature as low as 80 ℃ (at ambient pressure) allowed the direct formation of $BaTiO_3$ from titanium alkoxides and barium hydroxide solutions in the presence of aqueous KOH[57]. Subsequently, the hydrothermal method has been reported to prepare various $BaTiO_3$ by controlling the reaction temperature, reaction solvent and morphology of TiO_2. Furthermore, the hydrothermal synthesis mechanisms of $BaTiO_3$, such as two main mechanisms of "*in situ* reaction mechanism" and "dissolution mechanism precipitation reaction mechanism", have been studied. In addition to $BaTiO_3$, perovskites of other A-site metals (Ca, Sr, Pb) can also be prepared in one step under hydrothermal conditions. Wei et al. showed that by using solvothermal conditions with ethylenediamine and ethanolamine as solvents, $Ba_{1-x}Sr_xTiO_3$ could be obtained with well-formed nanocrystals and shapes varying from cube-like to spherical[58]. Others such as zirconates, niobates, and tantalates can also be synthesized by hydrothermal/solvothermal method. Kumada et al. found that for $KNbO_3$ three possible crystal symmetries, orthorhombic, tetragonal and cubic, could be formed, depending on the reaction temperature and the ratio of KOH/Nb_2O_5[59]. Although some materials have been synthesized by this method, there is still a need to explore the hydrothermal synthesis of perovskite oxides with more compositional and structural diversity.

2.3.3 Thin Film Synthesis Method

In order to investigate the structure-activity relationship of perovskite oxide electrocatalysts, some thin film growth techniques have been developed, including pulse laser deposition and molecular beam epitaxy. Pulsed laser deposition is a method of bombarding objects with lasers, and then depositing the bombarded materials on different substrates to obtain deposits or thin films. In this way, the thin film samples with a definite surface, single crystal orientation and definite strain state can be obtained. This type of materials eliminate the influence of these factors on the activity of oxide powder, allowing to better measure the intrinsic activities of these oxide surfaces. Stoerzinger et al. prepared $LaCoO_3$ thin films (10 nm in thickness) by pulsed laser deposition on different substrates[60]. Due to the lattice mismatch between the $LaCoO_3$ thin film and the substrate, a moderate tensile strain was generated, which could induce the change of electronic structure and lead to an increase of activity. Weber et al. performed the epitaxial growth of [001]-oriented $La_{0.6}Sr_{0.4}CoO_3$ (LSCO) films with a thickness of 100 nm on the surface of $NdGaO_3$ by pulse laser deposition[61]. This thin film material is an excellent model for studying the structure-activity relationships such as surface orientation and interatomic distance (epitaxial strain) in cobalt oxide catalysts. They used X-ray photoelectron spectroscopy (XPS) to reveal the degradation process of the thin film material under dynamic conditions, which involves cation leaching and oxide phase transition, and they observed surface stoichiometric changes and the formation of cobalt hydroxide.

Molecular beam epitaxy is a newly developed method for fabrication of perovskite films. In ultra-high vacuum environment, high quality thin film materials can be produced by projecting the atoms or molecular beams generated by thermal evaporation onto a substrate with a certain orientation. The advantages of this technology include low substrate temperature, easy precise control of beam strength, controllable film composition and doping concentration. Using this technique, it has been possible to produce single crystal perovskite films as thin as tens of atomic layers. Tang et al. synthesized single crystalling epitaxy $SrIrO_3$(100) using molecular beam epitaxy on $DyScO_3$(110) substrates and found that $SrIrO_3$ films were an order of magnitude more active than

IrO_2[62]. Wang et al. accurately synthesized a series of $LaNi_{1-x}Fe_xO_3$ (LNFO) thin films by molecular beam epitaxy and investigated the effects of Fe substitution on the lattice structure, electronic property and OER activity of the obtained thin films[63]. They found that LNFO with 37.5% Fe substitution had the best OER catalytic activity.

The above studies have highlighted the great achievements being made toward the preparation of perovskite oxides. When used as electrocatalysts, the morphology, specific surface area, particle size and crystal structure have great effects on catalytic performance of perovskite oxides. Hence, optimization of preparation methods is important to meet these use requirements of perovskite electrocatalysts[64,65]. Meanwhile, the development of simple and large-scale methods to obtain high purity perovskite electrocatalysts has practical application value.

3 Recent Advances of PerovskiteType Water Oxidation Electrocatalysts

3.1 Electrocatalysts in Alkaline Media

Water oxidation in alkaline media is closely related to the alkaline water electrolysis technology. Since the oxygen electrocatalytic activity of $LaCoO_3$ was first proposed by D. B. Meadowcroft[18], multiple perovskite-type water oxidation catalysts containing different transition metals (*e.g.*, Mn, Fe, Ni and Cu) were reported successively. In order to reveal the activity trend, Rossmeisl et al. calculated and compared the theoretical activities of various perovskite-type water oxidation electrocatalysts based on density functional theory (DFT)[66]. The authors found that the theoretical overpotentials of these electrocatalysts show the volcano-shaped dependence on the Gibbs free energy of adsorbed oxygen species (*i.e.*, $\Delta G_{O^*}-\Delta G_{HO^*}$), as shown in Figure 9a. The corresponding perovskite-type elec-

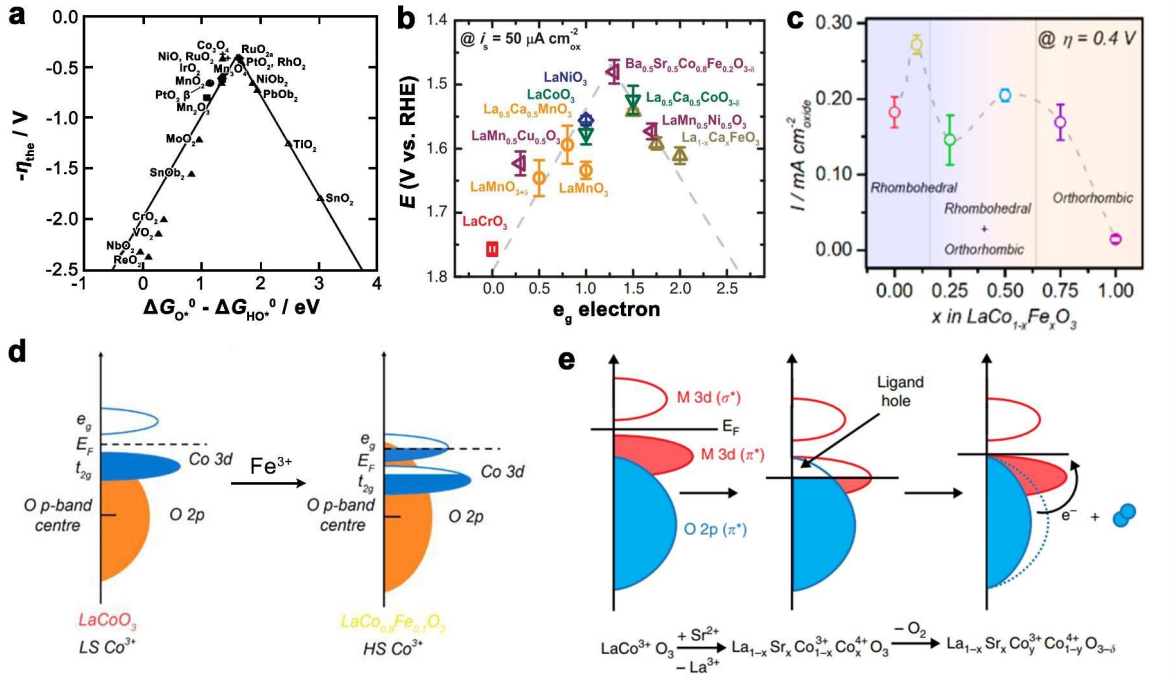

Figure 9 (a) The volcano-shaped dependence of theoretical overpotentials on ΔG_{O^*}-ΔG_{HO^*}. (a) Reprinted with permission from Ref. [66]. Copyright 2021, Wiley-VCH. (b) The volcano relationship between OER intrinsic activity and the e_g orbital filling of B cations in ABO_3. (b) Reprinted with permission from Ref. [19]. Copyright 2011, American Association for the Advancement of Science. (c) Specific activities of $LaCo_{1-x}Fe_xO_3$ at 1.63 V. (d) Schematic representation of Co 3*d*-O 2*p* overlap for $LaCoO_3$ and $LaCo_{0.9}Fe_{0.1}O_3$. (c, d) Reprinted with permission from Ref. [69]. Copyright 2017, American Chemical Society. (e) Correlation between Co-O bond covalency and oxygen vacancy concentration for $La_{1-x}Sr_xCoO_{3-\delta}$. (e) Reprinted with permission from Ref. [70]. Copyright 2016, Nature Publishing Group.

trocatalysts exhibit OER activity in the order: $SrCoO_3$ > $LaNiO_3$ > $SrNiO_3$ > $SrFeO_3$ > $LaCoO_3$ > $LaFeO_3$ > $LaMnO_3$. Among them, $SrCoO_3$ is closest to the volcano peak. This indicates that its binding energy between catalyst and adsorbed intermediate is moderate, *i.e*., neither too strong nor too weak, resulting in the optimal OER activity. The descriptor ΔG_{O^*}-ΔG_{HO^*} originates from the Sabatier principle, and is consistent with the results reported by Bockris et al.[45] and Matsumoto et al[67].

The perovskite-type water oxidation electrocatalyst actually attracted attentions since the discovery of $Ba_{0.5}Sr_{0.5}Co_{0.8}Fe_{0.2}O_{3-\delta}$ (BSCF) catalyst, which has an order of magnitude higher intrinsic activity than state-of-the-art IrO_2 catalyst[19]. By combining theory with experiment, the authors demonstrated a volcano relationship between intrinsic activity and the e_g orbital filling of perovskite-type water oxidation electrocatalyst (Figure 9b). The perovskite-type oxide with e_g occupancy close to 1 tends to possess superior OER activity, and this theoretical descriptor also applies to multiple electrocatalysts, such as $Ca_2MN_2O_5$[68] and $CaCu_3Fe_4O_{12}$[29].

Although several activity descriptors have been successfully established, they are not sufficient to guide researchers in designing and synthesizing electrocatalysts to meet industrial demands. The perovskite-type water oxidation electrocatalyst used in practical application requires better activity, stronger stability and superior conductivity. These can be achieved by experimentally optimizing their intrinsic activity and apparent activity. The former is strongly related to the electronic structure of catalyst, and can be accomplished by adjusting the composition and crystal structure. It makes the latter possible by increasing the number of accessible active site, such as constructing nanostructure and forming composite. Progress has been made in enhancing the water oxidation catalytic performance of perovskite-type electrocatalysts through the above optimization strategies.

Benefited from the flexible chemical compositions, modulating the composition of perovskite-type electrocatalysts is a common method to enhance the water oxidation catalytic performance. The relevant way can be classified into A-site, B-site, and oxygen modulation, who share a general formula as $A_{1-x}A'_xB_{1-y}B'_yO_{3\pm\delta}$. Among these, B-site modulation will directly affect the OER activity, because the B sites, occupied by transition metals, usually act as the active sites for catalysis. For instance, Duan et al. replaced partial Co in $LaCoO_3$ by Fe, and synthesized a series of $LaCo_{1-x}Fe_xO_3$ (x = 0, 0.1, 0.25, 0.50, 0.75, 1.00)[69]. They found that 10at% Fe substitution makes CO^{3+} in $LaCoO_3$ exhibit a higher spin state, and then enhances the hybridization between Co (e_g orbital) and O (p orbital), resulting in the best water oxidation electrocatalytic activity (Figure 9c, d). Moreover, there is often a bimetallic synergistic effect between the cations B′ and B. For example, the role of iron in cobalt-based and nickel-based catalyst systems has been long recognized. Suntivich et al. developed this classic bimetallic synergy into perovskite type oxide and synthesized the classic electrocatalysts, such as BSCF and $La_{0.2}Sr_{0.8}Co_{1-x}Fe_xO_{3-\delta}$ (LSCF)[19].

In most cases, the A-site element will not participate in the water oxidation process, but A-site modulation is able to tune the electronic structure of B site or O site, thereby indirectly affecting the OER activity of perovskite-type electrocatalyst. For example, Mefford et al. synthesized La_{1-x} $Sr_xCoO_{3-\delta}$ by partially substituting of La for Sr[70]. They found that the Sr^{2+} substitution in La_{1-x} $Sr_xCoO_{3-\delta}$ will increase oxidation state of Co, strengthen the covalency of Co-O bond, and create oxygen vacancies, which improve the redox activity of lattice oxygen species, thereby boost the water oxidation catalytic performance (Figure 9e).

Anion doping is also an effective optimization strategy, attributing to the optimization of conductivity and electronic structure in pristine perovskites. For example, Hua et al. synthesized a fluorine doped perovskite-type oxide (labeled as $La_{0.5}Ba_{0.25}Sr_{0.25}CoO_{2.9-\delta}$-$F_{0.1}$)[71]. They suggested that the F-anion doping can activate the lattice oxygen, promote the proton/electron transfer, and regulate the desorption energy related to Co-OO* bond, which together enhance the

water oxidation electrocatalytic performance.

The crystal structure of perovskite-type oxide has an inseparable connection with the relevant electrocatalytic performance. As mentioned above, a simple perovskite-type oxide could exhibit diverse crystal phases, known as polymorphs. Although they share the identical nominal composition, their geometric coordination environments and electronic structures in an atomic scale are distinguishing, which tend to invest significantly different activities and stabilities. For example, Li et al. prepared $LaMnO_3$ nanosheets with orthorhombic, tetragonal and hexagonal phases by varying the calcination time[53]. Among these, orthorhombic $LaMnO_3$ showed the best OER performance, which can be attributed to its unique electronic structure, including e_g filling, hybridization degree, and surface oxygen vacancies (Figure 10a, b).

Cao et al. prepared a series of R-P phase nickelates $La_nSrNi_nO_{3n+1}$(n = 1, 2, 3, and ∞) to investigate the role of dimensionality on the electronic structure and OER activity in perovskite-type structure[72]. The experimental results showed that the OER activity of R-P phase electrocatalyst was improved with the increase of the dimensionality (Figure 10c). They believed that the increase of dimensionality renders the expansion of Ni 3*d* band, accompanying by the insulator-to-metal transition and stronger Ni-O hybridization (Figure 10d). The resulting high conductivity and optimized hybridization will accelerate the OER kinetics.

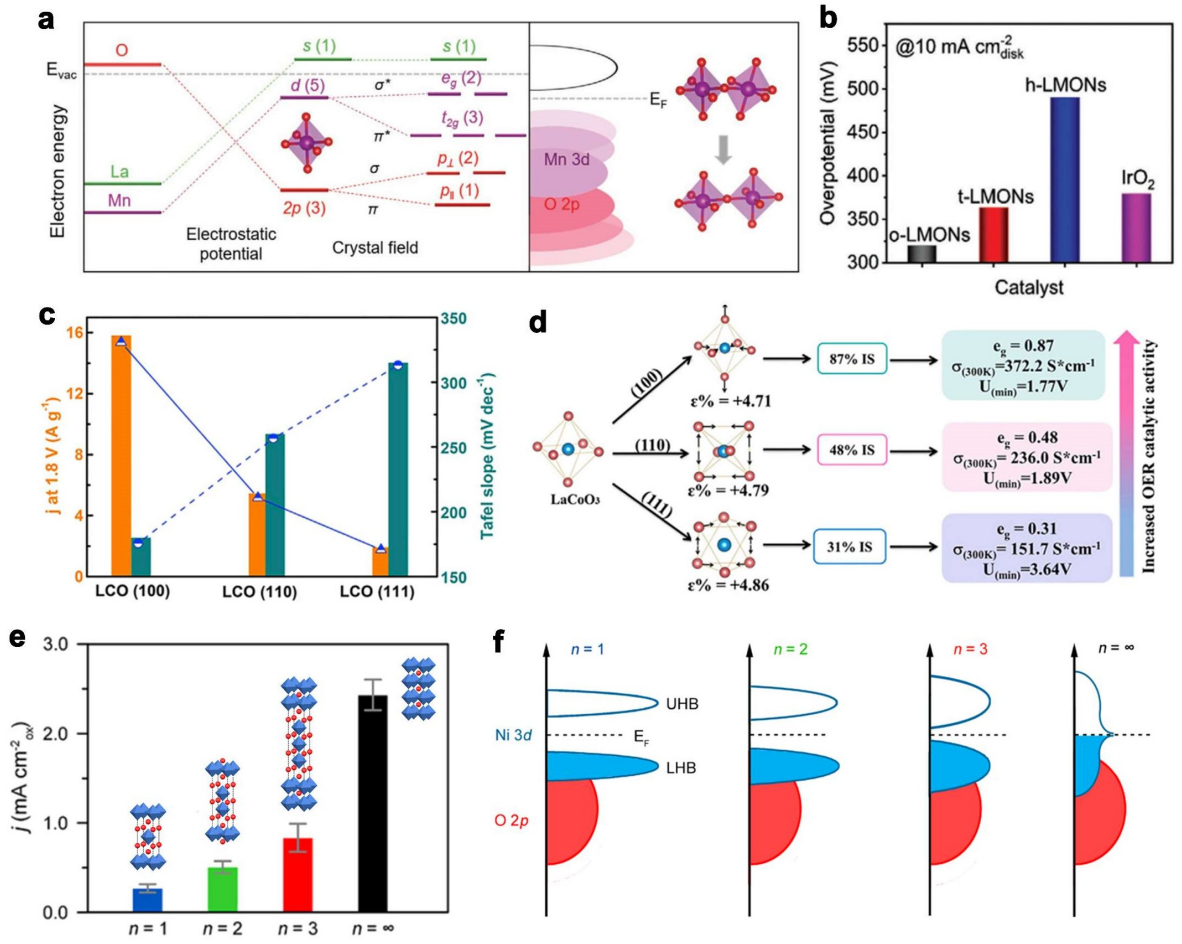

Figure 10 (a) Schematic electronic structure of $LaMnO_3$. (b) Comparison of overpotentials @ 10 mA·cm^{-2} for $LaMnO_3$ nanosheets with different crystal phases. (a, b) Reprinted with permission from Ref. [53]. Copyright 2021, Wiley-VCH. (c) Comparison of specific activities at 1.67 V, (d) schematic band structures for $La_nSrNi_nO_{3n+1}$ (n = 1, 2, 3, and ∞). (e, f) Reprinted with permission from Ref. [72]. Copyright 2020, American Chemical Society. (color on line)

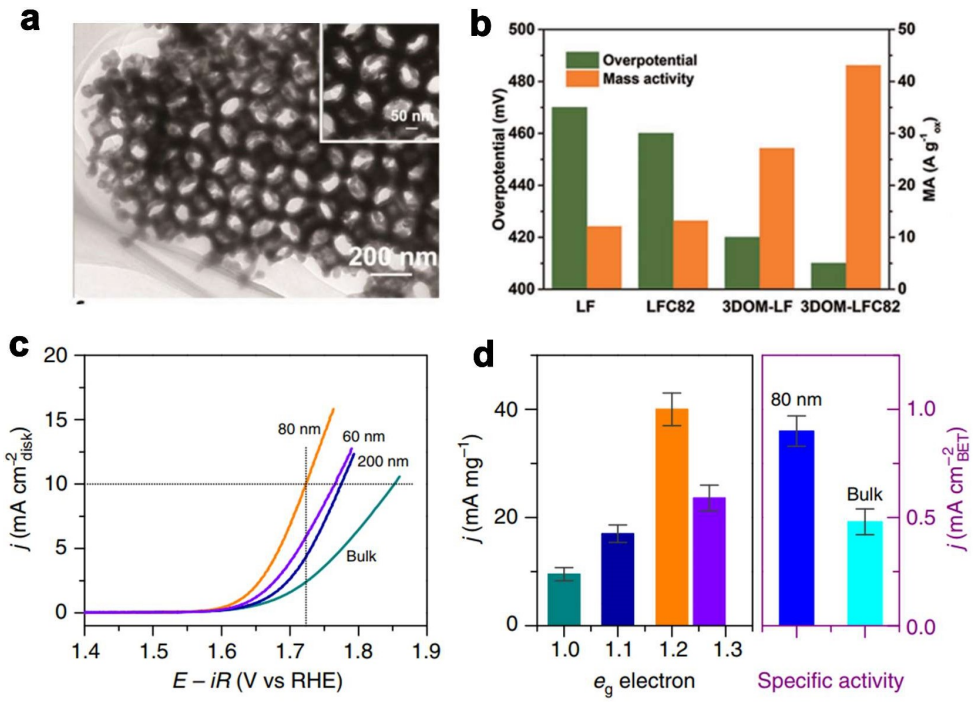

Figure 11 (a) Morphology of 3DOM-LFC82. (b) Comparisons of overpotentials @ 10 mA·cm^{-2} and mass activities @ η = 400 mV of 3DOM-LFC82 and catalysts without Co and/or 3D ordered microporous. (c) Polarization curves, (d) mass activities and special activities at overpotential = 490 mV of $LaCoO_3$ with different particle sizes. (a, b) Reprinted with permission from Ref. [73]. Copyright 2018, Wiley-VCH. (c, d) Reprinted with permission from Ref. [74]. Copyright 2016, Nature Publishing Group.

Nanostructure construction is one of the common design strategies, which is necessary for perovskite-type electrocatalysts to adapt the demands of practical applications. The perovskite-type materials synthesized by traditional methods (*e.g.*, solid-state method, decomposition method and coprecipitation method) usually have irregular morphology, large particle size, and small surface area. These features restrict the catalytic activity and commercial application of perovskite-type oxide. Thus, researchers have devoted considerable efforts to tailor the nanoscale morphology of perovskite-type materials. For example, Dai et al. first reported perovskite-type electrocatalyst $LaFe_{0.8}Co_{0.2}O_3$ with 3D ordered macroporous (3DOM-LFC82) using the colloidal crystal template method (Figure 11a)[73]. The unique 3DOM architecture contributes to the enhancement of OER activity for the higher surface area (Figure 11b), and better charge/mass transport ability. Moreover, it also facilitates the escape of gaseous oxygen and inhibits the degradation of Nafion ionomer, thus endowing 3DOM-LFC82 the enhanced stability.

Nanotechnology in material design not only limits tailoring the external morphology, but also triggers the variation of internal electronic structure due to the unique size effect of nanomaterials. For instance, the controllable regulation of eg orbital configuration in Co^{3+} can be achieved by reducing the size of $LaCoO_3$. Zhou et al. synthesized a series of $LaCoO_3$ with different particle sizes, and they confirmed that there is a size-induced spin-state transition from low spin ($t_{2g}^6e_g^0$) to high spin ($t_{2g}^4e_g^2$) for 80 nm $LaCoO_3$[74]. The higher spin state increases the e_g orbital filling in Co^{3+} to the ideal value of 1.2, leading the 80 nm $LaCoO_3$ to exhibit the best OER activity (Figure 11c, d). In spite of the development of various efficient water oxidation electrocatalysts, their catalytic mechanisms are still the pending issues. There are two kinds of widely accepted mechanisms of OER catalysis, including adsorbate evolution mechanism (AEM) and lattice oxygen-mediated (LOM). AEM is conventionally assumed as a four-proton-electron coupled transfer path-

way, in which the catalyst provides active adsorption sites (M sites), and the generated O_2 is totally originated from electrolyte. For an example of OER in an alkaline medium (Figure 12a), the reaction pathways can be described by the following equations[66, 75, 76]:

$$M + OH^- \rightarrow M\text{-}OH + e^- \quad (2)$$

$$M\text{-}OH + OH^- \rightarrow M\text{-}O + H_2O + e^- \quad (3)$$

$$M\text{-}O + OH^- \rightarrow M\text{-}OOH + e^- \quad (4)$$

$$M\text{-}OOH + OH^- \rightarrow M + O_2 + H_2O + e^- \quad (5)$$

With the development of advanced characterization technology, researchers have recently found that the OER catalytic mechanism is not limited to AEM, and the lattice oxygen of catalyst may also participate in it. This catalytic mechanism is defined as LOM. Three possible LOM reaction pathways extracted from recently researches are elucidated in Figure 12b-d, which differ in bonding manner of lattice oxy gen and adsorbed oxygen intermediates[70, 77, 78].

The main difference between AEM and LOM, apart from the source of the O_2 product, is that LOM often involves non-concerted proton-electron-transfer processes, such as O-O coupling step. Therefore, LOM can break the conventional scaling relationship of AEM and possess lower reaction barriers, which will accelerate the OER catalytic course. It is worth noting that although the water oxidation catalysts following LOM possess higher catalytic activity, they also tend to show worse structurally stabilities, which behave of suffering adverse structure evolutions (e.g., cation leaching, surface reconstruction, particle aggregation, and oxidative degradation)[79, 80]. These will lead to the uncertain active phase and catalytic mechanism, invalidating the established descriptors or principles. The most typical example for perovskite-type catalyst is BSCF, which triggers the LOM mechanism, breaks the scaling relationship of AEM, and boosts the OER kinetics. However, it also accelerates the dissolution of cations, such as Ba^{2+}, Sr^{2+}, CO^{2-3+} and Fe^{2-3+}. The former two cations are soluble in the electrolyte, while the transition metal cations will be dissolved and redeposited on the surface of BSCF, forming an amorphous CoFe (oxy)hydroxide layer[80].

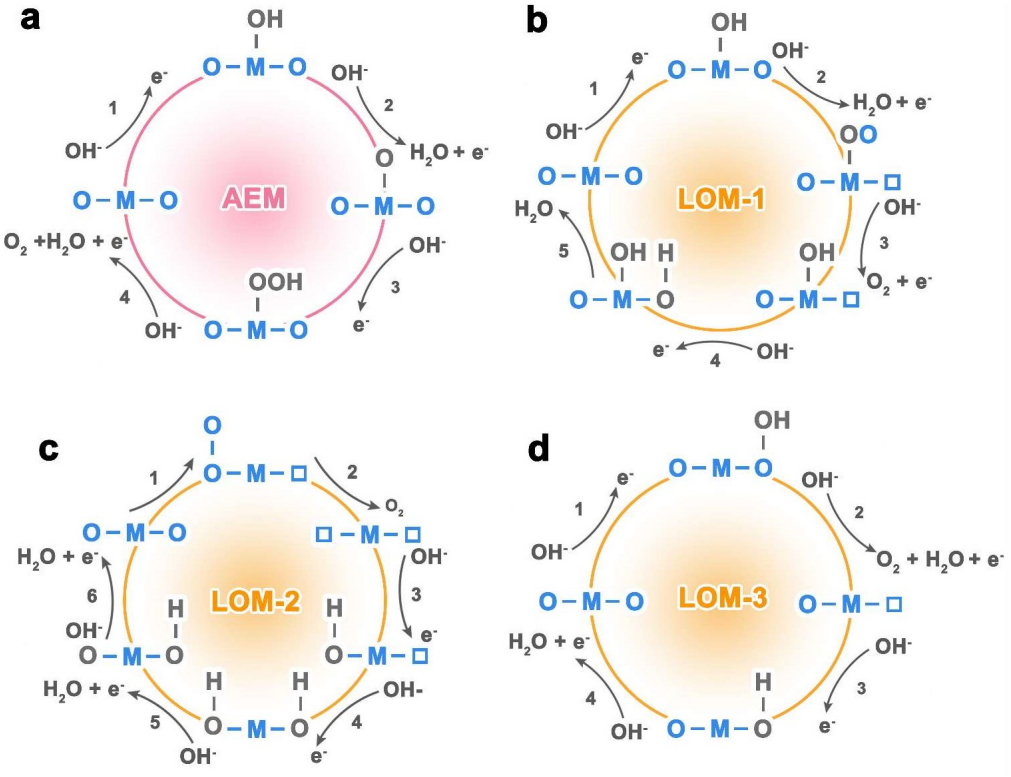

Figure 12 Schematic illustrations for the reaction pathways of (a) AEM and (b-d) three possible LOMs (labelled as LOM-1, LOM-2, LOM-3).

Since the actual active phase is not BSCF, the conventional AEM mechanism and the descriptor originating from it (*i.e.*, e_g orbitals filling) are no longer applicable. Nevertheless, the original structure of perovskite-type electrocatalyst fundamentally affects the amorphous phase derived from it. Furthermore, it has been recognized that a universal inverse correlation between OER activity and structural stability exists, *i.e.*, the electrocatalyst with higher activity often exhibits poorer structural stability[81]. This is because the water oxidation reaction pathway of such electrocatalyst often follows the LOM mechanism with rapid kinetics. However, the spill-over of lattice oxygen tends to destabilize the structural framework, leading to electrocatalyst deactivation. Therefore, it is necessary to balance the inverse relationship for the development of next-generation water oxidation catalysts with the improved both activity and stability.

3.2 Electrocatalysts in Acidic Media

Severe acidic and strong oxidation conditions of proton exchange membrane water electrolyzers (PEMWEs) limit the selection range of water oxidation catalysts, which must be Ir or Ru-based catalysts. Due to the poor stability of Ru-based catalysts, IrO_2 is a compromise choice between activity and stability. However, the rapidly increasing cost of Ir has greatly hindered the practical application of PEMWEs[82, 83]. This requires that the intrinsic activity and stability of novel Ir-based catalysts must be improved to surpass IrO_2. On the other hand, the utilization of Ir needs to

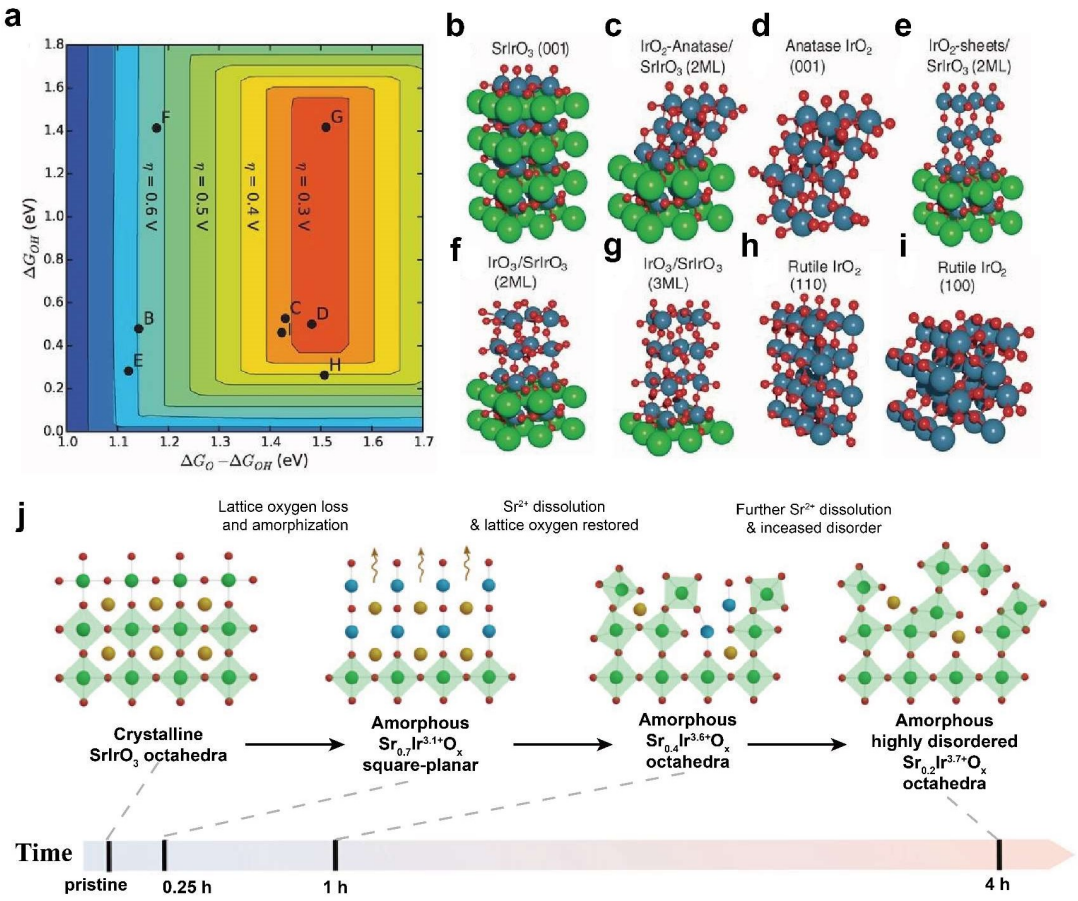

Figure 13 (a) Theoretical overpotential volcanic plot based on scaling relation of 3C-$SrIrO_3$ system. (b-i) Surface models of IrO_x and 3C-$SrIrO_3$, where (b-i) correspond to (B-I) in the volcano plot in (a). (a-i) Reprinted with permission from Ref. [20]. Copyright 2016, American Association for the Advancement of Science. (j) Structural transformation from crystalline to amorphous surface of 3C-$SrIrO_3$. Reprinted with permission from Ref. [85]. Copyright 2021, American Association for the Advancement of Science. (color on line)

be increased to achieve greater economic benefits[84]. Perovskite-type oxides are a kind of very promising material to meet the above requirements. Its diverse composition and structure can effectively dilute Ir to improve mass activity, while enhancing Ir intrinsic activity through potential synergistic and structural effects.

$SrIrO_3$ has become the most widely studied perovskite material for acidic water oxidation due to its high activity, excellent stability and low Ir mass fraction. It was first proposed as a pseudo-cubic perovskite structure (3C-$SrIrO_3$) synthesized by pulsed laser deposition, in which all IrO_6 octahedra are cornershared[20]. In a continuous 30-hour testing, it had only 270 to 290 millivolts of overpotential. However, the authors found that 3C-$SrIrO_3$ experienced severe Sr leaching (up to 30% ~ 50% in the first 30 min) during testing, resulting in the surface amorphization. Therefore, the formation of IrO_x on the surface is considered to be responsible for the high catalytic activity of 3C-$SrIrO_3$. They simulated the 3C-$SrIrO_3$ surface models of Sr leaching in detail through DFT calculation (Figure 13a-i), and proposed that this IrO_x may have a structural motif of IrO_3 or anatase phase IrO_2. Another work further explored the information about the structural evolution of 3C-$SrIrO_3$ during electrochemical operation, *i.e.*, the interface transition from crystal structure to amorphous structure (Figure 13j)[85]. Their results showed that OER triggered the activation of lattice oxygen, which in turn initiated the coupling diffusion of Sr^{2+} and O^{2-} at the oxide-electrolyte interface, resulting in the formation of the ~ 2.4-nm-thick amorphous Sr_yIrO_x film. This amorphous structure consisted of highly disordered $Ir^{4+}O_6$ octahedra with Sr^{2+} and Ir^{3+} residues, and was speculated to have an open romanechite- or hollandite-like structures.

There are several crystalline phases of $SrIrO_3$, and

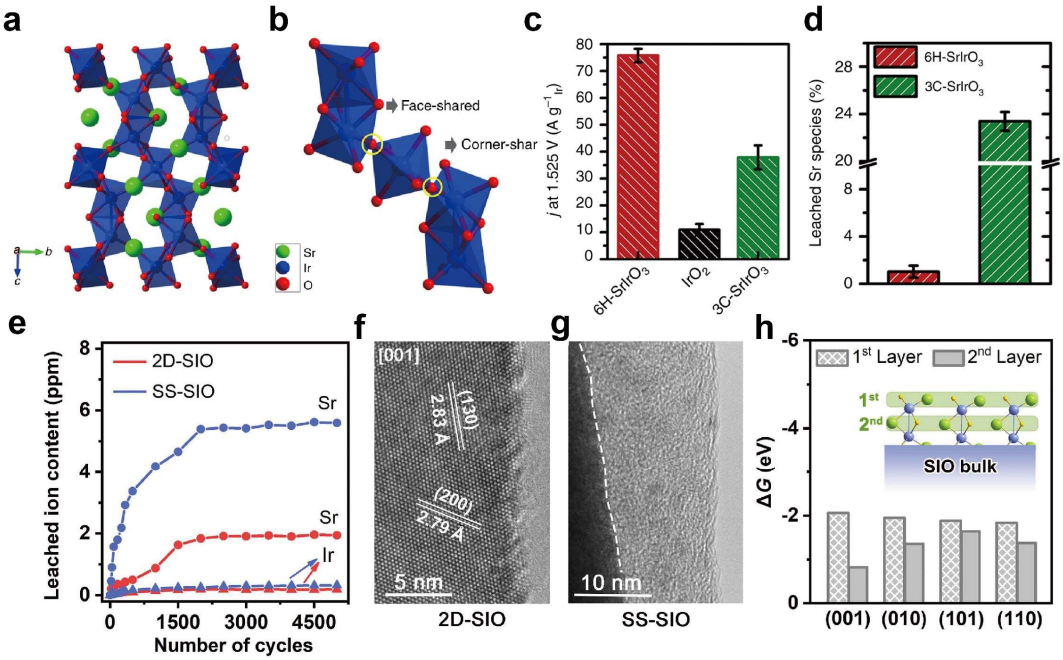

Figure 14 (a) Crystal structure of 6H-$SrIrO_3$. (b) A local connection pattern of IrO_6 octahedra in 6H-$SrIrO_3$. (c) Mass activity comparison of 6H-$SrIrO_3$, IrO_2 and 3C-$SrIrO_3$ normalized by Ir mass at 1.525 V vs. RHE. (d) Percentage of Sr leaching from 3C-$SrIrO_3$ and 6H-$SrIrO_3$ after 30-h catalytic stability test. (a-d) Reprinted with permission from Ref. [86]. Copyright 2018, Springer Nature. (e) Contents of Sr leaching for 2D-SIO and SS-SIO after 5000 cycles of linear sweep voltammetric (LSV) tests. The high resolution transmission electron microscopic (HRTEM) images of (f) 2D-SIO and (g) SS-SIO after the OER measurements. (h) ΔG plot of Sr leaching process in the first and second atomic layers on different $SrIrO_3$ surfaces. (e-h) Reprinted with permission from Ref. [87]. Copyright 2021, Elsevier. (color on line)

3C-$SrIrO_3$ is only a thermodynamically metastable phase. Our research group selectively synthesized 3C-$SrIrO_3$ and monoclinic $SrIrO_3$ (6H-$SrIrO_3$), and found that 6H-$SrIrO_3$ was a more thermodynamically stable phase (Figure 14a)[86]. Its Ir-O framework was composed of alternating face-sharing IrO_6 octahedral dimers and corner-sharing, isolated IrO_6 octahedral along the *c* axis (Figure 14b). In order to distinguish the difference between the two $SrIrO_3$ and explore the essential influence of different structures on catalysis, the OER performances of 6H-$SrIrO_3$ and 3C-$SrIrO_3$ were comprehensively compared. The experimental results showed that the mass activity of 6H-$SrIrO_3$ was twice that of 3C-$SrIrO_3$, and it had better catalytic stability (Figure 14c). More importantly, we found that 6H-$SrIrO_3$ had less Sr leaching (Figure 14d), and TEM images indicated that it maintained higher crystallinity before and after catalysis. Further theoretical calculations proved that its unusual face-sharing IrO_6 octahedral dimers contributed significantly to its remarkable catalytic activity and structural stability. In addition to the crystal structure, the crystal facet has recently been identified as a key factor controlling the catalytic properties of $SrIrO_3$. Our group compared a 2D ultrathin {001}-faceted $SrIrO_3$ perovskite material (2D-SIO) with unoriented 6H-$SrIrO_3$ (SS-SIO) to further study the crystal facet effect[87]. Inductively coupled plasma mass spectrometric (ICP-MS) results showed that 2D-SIO had less Sr leaching, which was estimated to correspond to less than two surface atomic layers. This was consistent with the higher crystallinity of 2D-SIO (Figure 14f) and the amorphous layer of SS-SIO (Figure 14g). Based on this, we calculated the thermodynamic driving force of Sr leaching from the first and second atomic layers at different $SrIrO_3$ surfaces by DFT, where (001) surface had the smallest change of Gibbs free energy (ΔG) of the second layer Sr leaching (Figure 14h). At the same time, we found that especially for (001) surface, when a small amount of Sr was dissolved on the surface, the subsequent Sr leaching will be hindered, resulting in high structural stability. We further calculated the theoretical activity and electronic structure using this model of slight Sr leaching. The results revealed that the catalytic activity and long-term stability of the catalyst were significantly improved due to the special exposure facet.

Due to the diverse composition of perovskite, more complex perovskites have been developed to further dilute Ir. For example, Koper et al. reported a class of Ir-based double perovskite materials (Ba_2MIrO_6, with M = Y, La, Ce, Pr, Nd and Tb) that contained 32% less iridium than the most advanced benchmarking IrO_2 catalyst[47]. Another class of 12L-perovskites ($Ba_4MIr_3O_{12}$; M = Pr, Bi, Nb) even lower Ir content, with the most active $Ba_4PrIr_3O_{12}$ having 55% less Ir than IrO_2[88]. However, for perovskites containing rare earth elements at B-site, it is often found that these catalysts are accompanied by severe A-site and B-site element leaching. This instability calls into question the so-call low iridium of these catalysts. Geiger et al. investigated the dissolution behavior of different oxides in acidic water oxidation, and found that severe leaching of perovskite resulted in the formation of completely amorphous IrO_x with similar properties to electrochemically hydrated IrO_x[89]. Therefore, these catalysts are not really low-iridium catalysts.

Although catalytic factors have been proved to influence the activity and stability of perovskite through structural evolution, our group identified that neglected non-catalytic factors also play an important role. For a long time, the corrosion of perovskite, especially the dissolution of Ir, is often attributed to electrochemical effects. The Ir leaching from perovskite structures is accompanied by OER and is considered to be a long-time process. However, the recent work of our group has clarified the fact that the influence of chemical corrosion cannot be ignored in the dissolution of the B-site Ir of perovskite, which occurs in a relatively short period of time[90]. Taking six typical Ir-based double perovskites $A_2B'IrO_6$ as examples (A = Ba, Sr, La; B = Li, Ti, Co, Y, Pr), it was proved by ingenious experimental design (Figure 15a) that when perovskite contacted with an acid solution instantly (less than 5 s), other materials except Sr_2TiIrO_6 released considerable amounts of

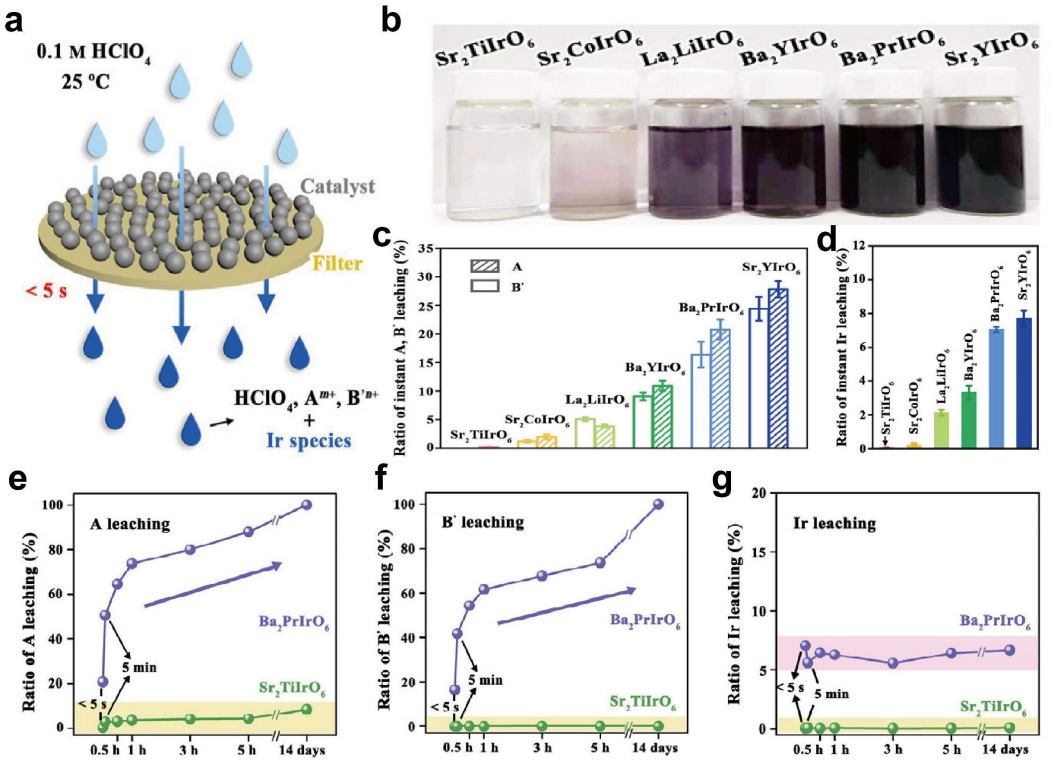

Figure 15 (a) Schematic of the instant acid corrosion test. (b) Photographs of $A_2B'IrO_6$ solutions after each instantaneous acid corrosion test. (c) Proportions of A-site and B′-site metals leached instantly from $A_2B'IrO_6$. (d) Proportion of Ir leached instantly from $A_2B'IrO_6$. (e) Proportions of A-site (e), B′-site (f) metals and Ir (g) leached from Sr_2TiIrO_6 and Ba_2PrIrO_6 during 14-day acid corrosion. (a-g) Reprinted with permission from Ref. [90]. Copyright 2022, Elsevier. (color on line)

A-site, B′-site metal and Ir (Figure 15b-d). At the same time, the instantaneous acid treatment resulted in the formation of amorphous layer on the surface similar to hydrated IrO_x, indicating that the surface reconstruction of perovskite had occurred before the catalysis. In addition, the dissolutions of A-site and B′-site metal were closely related to the acid treatment time. After a long time (14 days), the non-noble metals in Ba_2PrIrO_6 (as the representative of Sr_2CoIrO_6, La_2LiIrO_6, Ba_2YIrO_6 and Sr_2YIrO_6) were completely leached (Figure 15e, f) to form amorphous IrO_x, while the equilibrium of Ir dissolution was reached in a short time (Figure 15g). In contrast, Sr_2TiIrO_6 had only a slight cation leaching. Therefore, it can be determined that Ba_2PrIrO_6 was not really low iridium perovskite catalysts before catalysis, whereas Sr_2TiIrO_6 may be. Based on the above understanding, we supplemented the evaluation criteria of perovskite catalysts for future low-iridium catalysts, that is, the structural stability of perovskite to chemical corrosion must be taken into account.

In recent years, our group has developed a series of catalytically and structurally stable perovskite catalysts[91-94]. First, Ir was introduced into the catalytically inert and structurally stable parent material (*e.g.*, $SrTiO_3$, $SrZrO_3$) to form the perovskite solid solutions $SrTiO_3$-$SrIrO_3$ and $SrZrO_3$-$SrIrO_3$. These solid solu tions were found to easily form TiO_2-IrO_2 and ZrO_2-IrO_2 oxide solid solutions on the surface by leaching Sr under OER operating conditions. Detailed theoretical simulations showed that the anatase phase Ir oxide solid solution formed on the surface had ultra-high activity close to the theoretical overpotential volcano peak (Figure 17a, b), which was consistent with the experimental results. This suggests that the unique structure stabilized on the surface can improve the adsorption of OER oxygen-containing intermediates and thus enhance the activity. Further

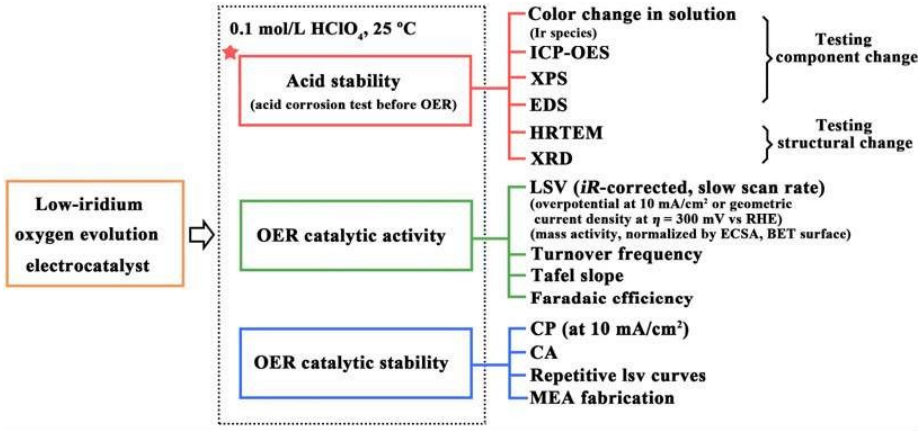

Figure 16 Experimental protocol for evaluating the performance of low Iridium oxygen evolution elec trocatalysts under acidic conditions. Reprinted with permission from Ref.[90]. Copyright 2022, Elsevier. (color on line)

studies of the electron structure indicated that the introductions of Ti and Zr were beneficial to optimize the hybridization of Ir 5*d* and O 2*p* orbitals through electron interaction (Figure 17c), and can stabilize the Ir site while optimizing the Ir-O bond strength (Figure 17d). Our group further reduced Ir content by synthesizing a class of triple perovskite catalysts with a general formula of $Ba_3M'M''_2O_9$ (M′ = Ti, In, or Zn; M''_2 = IrIr, IrTi, IrRu, or RuRu)[22]. The optimal $Ba_3TiIr_2O_9$ contained 47% less iridium than IrO_2, and gave 28 times higher activity. Our experimental and theoretical results showed that the face-shared Ir_2O_9 octahedral dimer was a necessary subunit for water oxidation to achieve reasonable catalytic activity and stability[95]. TiO_6 octahedra as an auxiliary subunit can modulate the covalent and oxygen p-band structure of the material to further improve the OER performances (Figure 17e). In short, we discover that the introduction of acid-stabilized metallic elements and the use of special crystal structures are effective ways to attain highly activity, long-term durability, and low-iridium catalysts.

Recent studies have shown that some 2D perovskite materials exhibit quite different properties from 3D perovskite in acid. Sr^{2+} of layered perovskite Sr_2IrO_4 is easily exchanged by H^+ to form protonated Ir oxide, while maintaining stable Ir-O framework[96]. This hydrated H_xIrO_y has been proved to be highly active, suggesting that a large number of protons contribute to the OER process. Due to the enrichment of H^+ between the layers, it is possible to exfoliate the few layers of Ir oxides from H_xIrO_y to form IrO_x thin sheets through the insertion of large organic bases. These unique properties make 2D perovskite a promising material and greatly broaden the research space of perovskite.

Compared with the extensive research on Ir-based perovskite, the development of Ru-based perovskite is still in its infancy. Although Ru-based catalysts generally have higher activity and lower cost, their poor stability has been the primary problem limiting their application. The reason for the lack of stability of Ru-based oxides may be that at high voltage (above 1.3 ~ 1.4 V), the Ru^{4+} changes to a higher valence state, and the Ru species with higher valence is easy to dissolve into the solution, leading to the decomposition of perovskite[97]. Therefore, it can be predicted that Ru-based perovskite degrades faster and becomes inactivated under the harsher operating voltage of PEMWEs. As one of the simplest Ru-based perovskites, $SrRuO_3$ is suitable for both theory and experiment as a good model, and the research focus is on how to stabilize the structure of $SrRuO_3$. The most common experimental means of stabilizing Ru site is doping, which is usually A-site. For example, Na or Ca substitution at the A site has been shown to enhance catalytic stability by regulating the electronic structure of the Ru site [98, 99]. In addition, Ji et al. also

used Sr leaching in $SrRuO_3$ to form RuO_2 clusters, thus significantly improving its catalytic stability and structural stability[100]. Other perovskites, such as quadruple $CaCu_3Ru_4O_{12}$, were found to be much more active and stable than RuO_2[101]. DFT calculations showed that this special structure effectively lowered the 4*d*-band center of the Ru site, thus weakening oxygen adsorption to enhance intrinsic activity. Although Ru-perovskite has made some progress, its stability has not been substantially improved to match that of IrO_2.

In summary, from the perspective of practical application to PEMWEs, we conclude that Ir-based perovskite is still the best choice at this stage due to the insufficient stability of Ru-based perovskite. The flexible structure and composition of Ir-based perovskite provide many opportunities for the modulation of catalysts with high OER performances. However, special attention on the corrosion behaviors of Ir-based perovskite (dissolutions of A-site metal and B-site Ir) should be paid , which has triggered a wide discussion on the structure-activity-stability relationships of perovskite. We emphasize the importance of analyzing the non-catalytic factors of Ir dissolution to understand the structural evolution of Ir-based perovskite. This would allow the actual low-iridium catalyst to be clarified. Based on the above understanding, a series of Ir-based perovskite catalysts containing Ti and Zr have been developed from our group, which are expected to be used in PEMWEs to replace IrO_2.

4 Conclusions and Perspectives

The development of highly active, stable and low-cost perovskite-type water oxidation electrocatalyst is an inevitable choice to promote the advance of multiple energy conversion and storage technologies. In this review, we summarize the crystal structures,

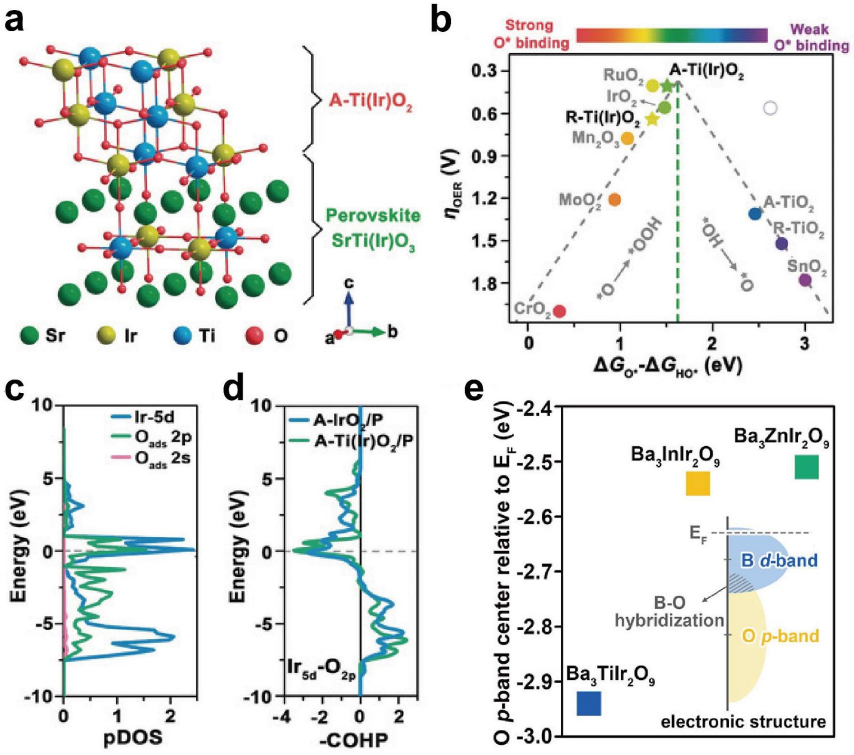

Figure 17 (a) Structural model of $SrTiO_3$-$SrIrO_3$ containing several atomic-layers of anatase Ti(Ir)O_2 (labeled A-Ti(Ir)O_2/P). (b) Theoretical overpotential volcanic plot of different oxide materials. (c) Calculated pDOS of oxygen-adsorbed A-Ti(Ir)O_2/P. (d) Calculated COHP of Ir5*d*-O2*p* bond for A-IrO_2/P ($SrIrO_3$ containing several atomic-layers of anatase IrO_2) and A-Ti(Ir)O_2/P. (a-d) Reprinted with permission from Ref. [92]. Copyright 2020, Wiley. (e) Calculated O *p*-band centers relative to the Fermi level of $Ba_3TiIr_2O_9$, $Ba_3InIr_2O_9$, and $Ba_3ZnIr_2O_9$. The inset in (e) illustrates the electronic structure of the metal *d*-band and O *p*-band hybridization of $Ba_3TiIr_2O_9$. Reprinted with permission from Ref. [22]. Copyright 2020, American Chemical Society. (color on line)

electronic properties, and synthetic chemistry of perovskite-type materials. The structure-activity relationship and the structural evolution mechanism of these catalysts are further discussed, by outlining the recent advances of perovskite-type water oxidation catalysts. However, exploiting the catalysts, which can meet the demands of advanced energy conversion and storage technologies, remains great challenges, thereby the further investigations must consider as follow (Figure 18).

(i) The precise synthesis is difficult for perovskite-type electrocatalyst. The precise synthesis of perovskite-type electrocatalysts with controlled morphology, tunable size and adjustable electronic structure is the prerequisite for the application of a perovskite-type oxide as an electrocatalyst. However, majority of the reported perovskite-type electrocatalysts are synthesized by solid-state method at high temperatures, which show large sizes and irregular morphology. Furthermore, each element in perovskite-type oxide exhibits different atomic sizes, oxidation states and electronegativities, the resulting different physical and chemical properties complicate the precise regulation of electronic structure. Therefore, it is of great practical significance to develop suitable synthetic methods and theoretical guideline for perovskite-type water oxidation electrocatalysts. Based on these, developing synthetic methods from a conventional solid-state method to a wet chemistry-assisted process (*e.g.*, sol-gel method and electrospinning) is crucial for optimizing the nanostructure of materials. On the other hand, the structural design principles can be constructed by combining experimental results and theoretical tools (*e.g.*, tolerance factor, formation energy, and phase diagram), and then guide the development of the synthesis methods for efficient perovskite-type electrocatalysts.

(ii) The long-term stability of perovskite-type water oxidation electrocatalyst needs careful evaluation. Activity, stability and cost are crucial for the practical applications of water oxidation electrocatalysts. However, the majority studies on perovskite-type electrocatalysts have concentrated on the improvements of OER activity and cost. The importance of stability is often underestimated, especially in acidic media. In fact, stability is the more important consideration in industry. The electrocatalysts with high activity rather poor stability will exhibit higher energy efficiency in the initial catalytic stage, but their activity will gradually decrease during the operation in years, shortening the service life of device. In contrast, in spite of the lower initial OER activity of electrocatalyst, it hardly decays during several years of operation. Then, its energy efficiency will beyond the former and maintain for several years. This example clearly shows the significance of long-term stability for water oxidation electrocatalysts in practical applications. In term of perovskite-type water oxida tion electrocatalysts, their high activity is often achieved at the expense of stability (*i.e.*, reversed relationship between activity and stability). Within a short time, the structural evolution, accompanying with the LOM mechanism, may not show the adverse effects on catalytic stability. However, the loss of active sites

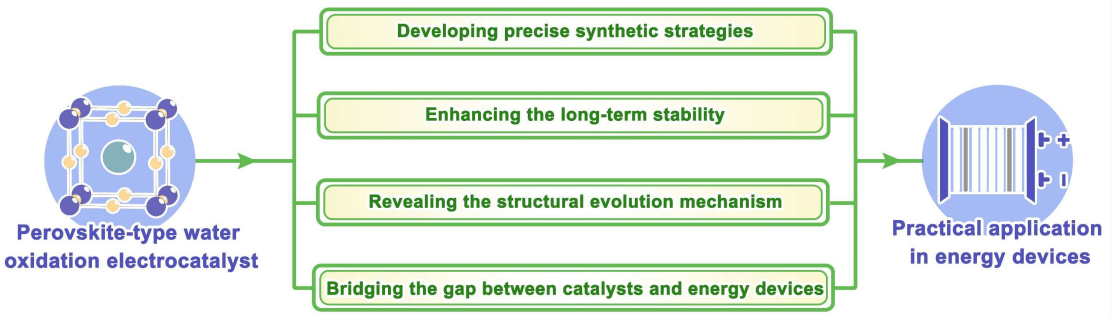

Figure 18 The research outlook for perovskite-type water oxidation electrocatalysts toward practical application in energy devices. (color on line)

and structural collapse will eventually deactivate the catalyst. Therefore, more attention should be paid to the long-term stability of perovskite-type water oxidation electrocatalyst.

(iii) The structural evolution mechanism of perovskite-type electrocatalyst is unclear. Perovskitetype water oxidation electrocatalysts often suffer from irreversible structural evolutions during the OER catalytic process, which result in the transformation of actual active phase from perovskite-type oxides to transition metal (oxy)hydroxide (in alkaline media) or hydrous IrO_x (in acidic media). Although this transformation sometimes generates higher catalytic activity, it comes at the expense of the structural stability, and even leads to deactivation of electrocatalyst. Therefore, in order to develop the highly active and stable perovskite-type electrocatalysts, we should gain further insight into their evaluation mechanisms under electrocatalysis conditions. However, the structural evolution, actual active phase and key intermediates are difficult to be monitored by conventional characterizations. The combination of electrochemical measurements and *in situ* characterizations are demanded. For example, the origin of product O_2 can be directly detected by using on line electrochemical mass spectrometry (OLEMS) coupling isotope labelling, and the OER reaction mechanism (AEM or LOM) can be deduced. The direct observations of structure transformation and surface reconstruction can be achieved by applying liquid transmission electron microscope. The electronic structure and local geometric coordination environment of material can be ascertained by *in situ* XAS. Therefore, it is necessary to reinforce the application of *in situ* characterizations to clearly understand the reaction mechanism of perovskite-type electrocatalysts, and then target the optimization strategy of activity and stability.

(iv) The gap between perovskite-type water oxidation catalysts and catalyst layers for energy devices should draw attention. Remarkable achievements have been made in the development of perovskite-type water oxidation catalysts, but nearly all of the reported materials are estimated by the lab-scale three-electrode system, rather in the membrane electrode assemblies (MEAs). In fact, none of these catalysts showed the as high activity and stability as they are assembled in the MEAs. In alkaline media, the mobility and diffusion coefficient of OH^- are much lower than those of H^+, and this disparity widens further in the anion exchange MEA. In addition, the chemical stability of anion exchange membrane and the structural stability of perovskite-type electrocatalysts should be enhanced. Therefore, there is still a long way to go for the application of perovskite-type water oxidation electrocatalyst in anion exchange membrane water electrolyzer (AEMWE). In acidic media, only iridium-based perovskite-type water oxidation catalysts can survive. Although their costs have been significantly reduced (compared with benchmark IrO_2), there are still shortcomings such as poor conductivity and stability, which will detriment the performance and life of PEMWE. Some researchers have stated the good activity and stability of certain catalysts by using lab-scale polymer membrane electrolyzer, majority of which are cm^2-scale PEMWE. However, whether the preparation of catalysts or the integration of MEA are difficult to be scaled up to meet the industrial demands. In general, researchers should spare no effort to solve the above problems to bridge the gap between perovskite-type water oxidation catalysts and catalyst layers for energy devices.

Acknowledgements:

X.Z. thanks for the financial support from National Natural Science Foundation of China (NSFC): Grant No. 21922507 and 22179046, and Jilin Province Science and Technology Development Plan (No. YDZJ202101ZYTS126). X. L. acknowledges the financial support from China Postdoctoral Science Foundation (No. 2021M701377).

References:

[1] Chu S, Majumdar A. Opportunities and challenges for a sustainable energy future[J]. Nature, 2012, 488(7411): 294-303.

[2] Trenberth K E, Cheng L J, Jacobs P, Zhang Y X, Fasullo J. Hurricane harvey links to ocean heat content and climate

change adaptation[J]. Earth's Future, 2018, 6(5): 730-744.

[3] Tang C, Zheng Y, Jaroniec M, Qiao S Z. Electrocatalytic refinery for sustainable production of fuels and chemicals [J]. Angew. Chem. Int. Ed., 2021, 60(36): 19572-19590.

[4] Chu S, Cui Y, Liu N. The path towards sustainable energy [J]. Nat. Mater., 2017, 16(1): 16-22.

[5] Yan Z F, Hitt J L, Turner J A, Mallouk T E. Renewable electricity storage using electrolysis[J]. Proc. Natl. Acad. Sci. U.S.A., 2020, 117(23): 12558-12563.

[6] De Luna P, Hahn C, Higgins D, Jaffer S A, Jaramillo T F, Sargent E H. What would it take for renewably powered electrosynthesis to displace petrochemical processes? [J]. Science, 2019, 364(6438): eaav3506.

[7] Beaudin M, Zareipour H, Schellenberglabe A, Rosehart W. Energy storage for mitigating the variability of renewable electricity sources: An updated review[J]. Energy Sustain. Dev., 2010, 14(4): 302-314.

[8] Hunter B M, Gray H B, Müller A M. Earth-abundant heterogeneous water oxidation catalysts[J]. Chem. Rev., 2016, 116(22): 14120-14136.

[9] Suen N T, Hung S F, Quan Q, Zhang N, Xu Y J, Chen H M. Electrocatalysis for the oxygen evolution reaction: recent development and future perspectives[J]. Chem. Soc. Rev., 2017, 46(2): 337-365.

[10] Hwang J, Rao R R, Giordano L, Katayama Y, Yu Y, Shao-Horn Y. Perovskites in catalysis and electrocatalysis[J]. Science, 2017, 358(6364): 751-756.

[11] Rose G. Ueber einige neue Mineralien des Urals[J]. J. Prakt. Chem., 2010, 19(1): 459-468.

[12] Chakhmouradian A R, Woodward P M. Celebrating 175 years of perovskite research: A tribute to Roger H. Mitchell[J]. Phys Chem Miner, 2014, 41(6): 387-391.

[13] Ortega-San-Martin L. Introduction to perovskites: A historical perspective[M]. New York: Springer, 2020. 1-41.

[14] Von Hippel A, Breckenridge R G, Chesley F G, Tisza L. High dielectric constant ceramics[J]. Ind. Eng. Chem., 1946, 6(4): 238-251.

[15] Bednorz J G, Müller K A Z. Possible high Tc superconductivity in the Ba-La-Cu-O system[J]. Z. Phys. B-Condensed Matter., 1986, 64(2): 189-193.

[16] Jonker G H, Santen J. Ferromagnetic compounds of manganese with perovskite structure[J]. Physica, 1950, 16(3): 337-349.

[17] Kojima A, Teshima K, Shirai Y, Miyasaka T. Organometal halide perovskites as visible-light sensitizers for photovoltaic cells[J]. J. Am. Chem. Soc., 2009, 131(17): 6050-6051.

[18] Meadowcroft D B. Low-cost oxygen electrode material [J]. Nature, 1970, 226(5248): 847-848.

[19] Suntivich J, May K J, Gasteiger H A, Goodenough J B, Shao-Horn Y. A perovskite oxide optimized for oxygen evolution catalysis from molecular orbital principles[J]. Science, 2011, 334(6061): 1383-1385.

[20] Seitz L C, Dickens C F, Nishio K, Hikita Y, Montoya J, Doyle A, Kirk C, Vojvodic A, Hwang H Y, Norskov J K, Jaramillo T F. A highly active and stable $IrO_x/SrIrO_3$ catalyst for the oxygen evolution reaction[J]. Science, 2016, 353(6303): 1011-1014.

[21] Xu X M, Zhong Y J, Shao Z P. Double perovskites in catalysis, electrocatalysis, and photo(electro)catalysis[J]. Trends Chem., 2019, 1(4): 410-424.

[22] Zhang Q, Liang X, Chen H, Yan W S, Shi L, Liu Y P, Li J Y, Zou X X. Identifying key structural subunits and their synergism in low-iridium triple perovskites for oxygen evolution in acidic media[J]. Chem. Mater., 2020, 32 (9): 3904-3910.

[23] Xu X M, Pan Y L, Zhong Y J, Ran R, Shao Z P. Ruddlesden-popper perovskites in electrocatalysis[J]. Mater. Horizons, 2020, 7(10): 2519-2565.

[24] Peña M A, Fierro J L G. Chemical structures and perfor mance of perovskite oxides[J]. Chem. Rev., 2001, 101(7): 1981-2017.

[25] George G. Fundamentals of perovskite oxides: Synthesis, structure, properties and applications[M]. Boca Raton: CRC Press, 2020.

[26] Tilley R. Perovskites structure-property relationships[M]. Chichester: John Wiley & Sons, 2016: 1-315.

[27] Rodríguez-Carvajal J, Hennion M, Moussa F, Mouden A H, Pinsard L, Revcolevschi A. Neutron-diffraction study of the Jahn-Teller transition in stoichiometric $LaMnO_3$[J]. Phys. Rev. B, 1998, 57(6): R3189-R3192.

[28] David W I F, Harrison W T A, Gunn J M F, Moze O, Soper A K, Day P, Jorgensen J D, Hinks D G, Beno M A, Soderholm L, Capone Ii D W, Schuller I K, Segre C U, Zhang K, Grace J D. Structure and crystal chemistry of the high-Tc superconductor $YBa_2Cu_3O_{7-x}$[J]. Nature, 1987, 327(6120): 310-312.

[29] Yagi S, Yamada I, Tsukasaki H, Seno A, Murakami M, Fujii H, Chen H, Umezawa N, Abe H, Nishiyama N, Mori S. Covalency-reinforced oxygen evolution reaction catalyst[J]. Nat. Commun., 2015, 6: 8249.

[30] Koo B, Kim K, Kim J K, Kwon H, Han J W, Jung W. Sr segregation in perovskite oxides: Why it happens and how it exists[J]. Joule, 2018, 2(8): 1476-1499.

[31] Goldschmidt V M. Die Gesetze der Krystallochemie[J]. Naturwissenschaften, 1926, 14(21): 477-485.

[32] King G, Woodward P M. Cation ordering in perovskites [J]. J. Mater. Chem., 2010, 20(28): 5785-5796.

[33] Ruddlesden S N, Popper P. The compound $Sr_3Ti_2O_7$ and its structure[J]. Acta Cryst., 1958, 11(1): 54-55.

[34] Dylla M T, Kang S D, Snyder G J. Effect of two-dimensional crystal orbitals on fermi surfaces and electron transport in three-dimensional perovskite oxides[J]. Angew. Chem. Int. Ed., 2019, 58(17): 5503-5512.

[35] Pesquera D, Herranz G, Barla A, Pellegrin E, Bondino F, Magnano E, Sánchez F, Fontcuberta J. Surface symmetry-breaking and strain effects on orbital occupancy in transition metal perovskite epitaxial films[J]. Nat. Commun., 2012, 3: 1189.

[36] Suntivich J, Gasteiger H A, Yabuuchi N, Nakanishi H, Goodenough J B, Shao-Horn Y. Design principles for oxygen-reduction activity on perovskite oxide catalysts for fuel cells and metal-air batteries[J]. Nat. Chem., 2011, 3 (7): 546-550.

[37] Lee Y L, Kleis J, Rossmeisl J, Shao-Horn Y, Morgan D. Prediction of solid oxide fuel cell cathode activity with first-principles descriptors[J]. Energy Environ. Sci., 2011, 4(10): 3966-3970.

[38] Grimaud A, May K J, Carlton C E, Lee Y L, Risch M, Hong W T, Zhou J G, Shao-Horn Y. Double perovskites as a family of highly active catalysts for oxygen evolution in alkaline solution[J]. Nat. Commun., 2013, 4: 2439.

[39] Hong W T, Stoerzinger K A, Lee Y L, Giordano L, Grimaud A, Johnson A M, Hwang J, Crumlin E J, Yang W L, Shao-Horn Y. Charge-transfer-energy-dependent oxygen evolution reaction mechanisms for perovskite oxides [J]. Energy Environ. Sci., 2017, 10(10): 2190-2200.

[40] Hong W T, Stoerzinger K A, Moritz B, Devereaux T P, Yang W L, Shao-Horn Y. Probing $LaMO_3$ metal and oxygen partial density of states using X-ray emission, absorption, and photoelectron spectroscopy[J]. J. Phys. Chem. C, 2015, 119(4): 2063-2072.

[41] Calle-Vallejo F, Inoglu N G, Su H Y, Martinez J I, Man I C, Koper M T M, Kitchin J R, Rossmeisl J. Number of outer electrons as descriptor for adsorption processes on transition metals and their oxides[J]. Chem. Sci., 2013, 4 (3): 1245-1249.

[42] Gerischer H. Electron-transfer kinetics of redox reactions at the semiconductor/electrolyte contact. A new approach [J]. J. Phys. Chem., 1991, 95(3): 1356-1359.

[43] Zaanen J, Sawatzky G A, Allen J W. Band gaps and electronic structure of transition-metal compounds[J]. Phys. Rev. Lett., 1985, 55(4): 418-421.

[44] Portier J, Poizot P, Tarascon J M, Campet G, Subramanian M. Acid-base behavior of oxides and their electronic structure[J]. Solid State Sci., 2003, 5(5): 695-699.

[45] Bockris J O, Otagawa T. The electrocatalysis of oxygen evolution on perovskites[J]. J. Electrochem. Soc., 1984, 131(2): 290-302.

[46] Kumar V, Kumar R, Shukla D K, Gautam S, Chae K H, Kumar R. Electronic structure and electrical transport properties of $LaCo_{1-x}Ni_xO_3$ ($0 \leqslant x \leqslant 0.5$)[J]. J. Appl. Phys., 2013, 114(7): 073704.

[47] Diaz-Morales O, Raaijman S, Kortlever R, Kooyman P J, Wezendonk T, Gascon J, Fu W T, Koper M T M. Iridium-based double perovskites for efficient water oxidation in acid media[J]. Nat. Commun., 2016, 7: 12363.

[48] Liu H, Ding X F, Wang L X, Ding D, Zhang S H, Yuan G L. Cation deficiency design: A simple and efficient strategy for promoting oxygen evolution reaction activity of perovskite electrocatalyst[J]. Electrochim. Acta, 2018, 259:1004-1010.

[49] Xu X M, Su C, Zhou W, Zhu Y L, Chen Y B, Shao Z P. Co-doping strategy for developing perovskite oxides as highly efficient electrocatalysts for oxygen evolution reaction[J]. Adv. Sci., 2016, 3(2): 1500187.

[50] Miao Y F, Wang X T, Zhang H J, Zhang T Y, Wei N, Liu X M, Chen Y T, Chen J, Zhao Y X. *In situ* growth of ultrathin perovskitoid layer to stabilize and passivate $MAPbI_3$ for efficient and stable photovoltaics[J]. eScience, 2021, 1 (1): 91-97.

[51] Zeng J, Bi L Y, Cheng Y H, Xu B M, Jen A K Y. Self-assembled monolayer enabling improved buried interfaces in blade-coated perovskite solar cells for high efficiency and stability[J]. Nano Res. Energy, 2022, 1: e9120004.

[52] Wang H, Wang L, Luo Q S, Zhang J, Wang C T, Ge X, Zhang W, Xiao F S. Two-dimensional manganese oxide on ceria for the catalytic partial oxidation of hydrocarbons[J]. Chem. Synth., 2022, 2(1): 2.

[53] Li Q, Wu J B, Wu T, Jin H R, Zhang N, Li J, Liang W X, Liu M L, Huang L, Zhou J. Phase engineering of atomically thin perovskite oxide for highly active oxygen evolution[J]. Adv. Funct. Mater., 2021, 31(38): 2102002.

[54] Jin C, Cao X C, Zhang L Y, Zhang C, Yang R Z. Preparation and electrochemical properties of urchin-like $La_{0.8}Sr_{0.2}MnO_3$ perovskite oxide as a bifunctional catalyst for oxygen reduction and oxygen evolution reaction[J]. J. Power Sources, 2013, 241: 225-230.

[55] Yu L J, Xu N, Zhu T L, Xu Z L, Sun M Z, Geng D. $La_{0.4}Sr_{0.6}Co_{0.7}Fe_{0.2}Nb_{0.1}O_{3-\delta}$ perovskite prepared by the sol-gel method with superior performance as a bifunctional oxygen electrocatalyst[J]. Int. J. Hydrogen Energy, 2020, 45

(55): 30583-30591.

[56] Wang Z, Li M, Liang C H, Fan L Q, Han J N, Xiong Y P. Effect of morphology on the oxygen evolution reaction for $La_{0.8}Sr_{0.2}Co_{0.2}Fe_{0.8}O_{3-\delta}$ electrochemical catalyst in alkaline media[J]. RSC Adv., 2016, 6(73): 69251-69256.

[57] Flaschen S S. An aqueous synthesis of barium titanate[J]. J. Am. Chem. Soc., 1955, 77(23): 6194-6194.

[58] Wei X, Xu G, Ren Z H, Wang Y G, Shen G, Han G R. Composition and shape control of single-crystalline $Ba_{1-x}Sr_xTiO_3$ (x=0-1) nanocrystals via a solvothermal route [J]. J. Cryst. Growth, 2008, 310(18): 4132-4137.

[59] Kumada N, Kyoda T, Yonesaki Y, Takei T, Kinomura N. Preparation of $KNbO_3$ by hydrothermal reaction[J]. Mater. Res. Bull., 2007, 42(10): 1856-1862.

[60] Stoerzinger K A, Choi W S, Jeen H, Lee H N, Shao-Horn Y. Role of strain and conductivity in oxygen electrocatalysis on $LaCoO_3$ thin films[J]. J. Phys. Chem. Lett., 2015, 6(3): 487-492.

[61] Weber M L, Baeumer C, Mueller D N, Jin L, Jia C L, Bick D S, Waser R, Dittmann R, Valov I, Gunkel F. Electrolysis of water at atomically tailored epitaxial cobaltite surfaces[J]. Chem. Mater., 2019, 31(7): 2337-2346.

[62] Tang R B, Nie Y F, Kawasaki J K, Kuo D Y, Petretto G, Hautier G, Rignanese G M, Shen K M, Schlom D G, Suntivich J. Oxygen evolution reaction electrocatalysis on $SrIrO_3$ grown using molecular beam epitaxy[J]. J. Mater. Chem. A, 2016, 4(18): 6831-6836.

[63] Wang L, Adiga P, Zhao J L, Samarakoon W S, Stoerzinger K A, Spurgeon S R, Matthews B E, Bowden M E, Sushko P V, Kaspar T C, Sterbinsky G E, Heald S M, Wang H, Wangoh L W, Wu J P, Guo E J, Qian H J, Wang J O, Varga T, Thevuthasan S, Feng Z X, Yang W L, Du Y G, Chambers S A. Understanding the electronic structure evolution of epitaxial $LaNi_{1-x}Fe_xO_3$ thin films for water oxidation[J]. Nano Lett., 2021, 21(19): 8324-8331.

[64] Ni L S, Guo R T, Fang S S, Chen J, Gao J Q, Mei Y, Zhang S, Deng W T, Zou G Q, Hou H S, Ji X B. Crack-free single-crystalline Co-free Ni-rich $LiNi_{0.95}Mn_{0.05}O_2$ layered cathode[J]. eScience, 2022, 2(1): 116-124.

[65] Li B, Li Z, Wu X, Zhu Z L. Interface functionalization in inverted perovskite solar cells: From material perspective [J]. Nano Res. Energy, 2022, 1(1): e9120011.

[66] Man I C, Su H Y, Calle-Vallejo F, Hansen H A, Martínez J I, Inoglu N G, Kitchin J, Jaramillo T F, Nörskov J K, Rossmeisl J. Universality in oxygen evolution electrocatalysis on oxide surfaces[J]. ChemCatChem, 2011, 3(7): 1159-1165.

[67] Matsumoto Y, Sato E. Electrocatalytic properties of transition metal oxides for oxygen evolution reaction[J]. Mater. Chem. Phys., 1986, 14(5): 397-426.

[68] Kim J, Yin X, Tsao K C, Fang S H, Yang H. $Ca_2MN_2O_5$ as oxygen-deficient perovskite electrocatalyst for oxygen evolution reaction[J]. J. Am. Chem. Soc., 2014, 136(42): 14646-14649.

[69] Duan Y, Sun S N, Xi S B, Ren X, Zhou Y, Zhang G L, Yang H T, Du Y H, Xu Z C J. Tailoring the Co 3*d*-O 2*p* covalency in $LaCoO_3$ by Fe substitution to promote oxygen evolution reaction[J]. Chem. Mater., 2017, 29(24): 10534-10541.

[70] Mefford J T, Rong X, Abakumov A M, Hardin W G, Dai S, Kolpak A M, Johnston K P, Stevenson K J. Water electrolysis on $La_{1-x}Sr_xCoO_{3-\delta}$ perovskite electrocatalysts [J]. Nat. Commun., 2016, 7: 11053.

[71] Hua B, Li M, Pang W Y, Tang W Q, Zhao S L, Jin Z H, Zeng Y M, Amirkhiz B S, Luo J L. Activating p-blocking centers in perovskite for efficient water splitting[J]. Chem, 2018, 4(12): 2902-2916.

[72] Cao C, Shang C Y, Li X, Wang Y Y, Liu C X, Wang X Y, Zhou S M, Zeng J. Dimensionality control of electrocatalytic activity in perovskite nickelates[J]. Nano Lett., 2020, 20(4): 2837-2842.

[73] Dai J, Zhu Y L, Zhong Y J, Miao J, Lin B W, Zhou W, Shao Z P. Enabling high and stable electrocatalytic activity of iron-based perovskite oxides for water splitting by combined bulk doping and morphology designing[J]. Adv. Mater. Interfaces, 2019, 6(1): 1801317.

[74] Zhou S M, Miao X B, Zhao X, Ma C, Qiu Y H, Hu Z P, Zhao J Y, Shi L, Zeng J. Engineering electrocatalytic activity in nanosized perovskite cobaltite through surface spin-state transition[J]. Nat. Commun., 2016, 7: 11510.

[75] Burke M S, Enman L J, Batchellor A S, Zou S H, Boettcher S W. Oxygen evolution reaction electrocatalysis on transition metal oxides and (oxy)hydroxides: Activity trends and design principles[J]. Chem. Mater., 2015, 27(22): 7549-7558.

[76] Bockris J O, Otagawa T. Mechanism of oxygen evolution on perovskites[J]. J. Phys. Chem. C, 1983, 87(15): 2960-2971.

[77] Grimaud A, Diaz-Morales O, Han B H, Hong W T, Lee Y L, Giordano L, Stoerzinger K A, Koper M T M, Shao-Horn Y. Activating lattice oxygen redox reactions in metal oxides to catalyse oxygen evolution[J]. Nat. Chem., 2017, 9(5): 457-465.

[78] Yoo J S, Rong X, Liu Y S, Kolpak A M. Role of lattice oxygen participation in understanding trends in the oxygen evolution reaction on perovskites [J]. ACS Catal., 2018, 8

(5): 4628-4636.

[79] Gao R Q, Deng M, Yan Q, Fang Z X, Li L C, Shen H Y, Chen Z F. Structural variations of metal oxide-based electrocatalysts for oxygen evolution reaction [J]. Small Methods, 2021, 5(12): 2100834.

[80] Fabbri E, Nachtegaal M, Binninger T, Cheng X, Kim B J, Durst J, Bozza F, Graule T, Schäublin R, Wiles L, Pertoso M, Danilovic N, Ayers K E, Schmidt T J. Dynamic surface self-reconstruction is the key of highly active perovskite nano-electrocatalysts for water splitting[J]. Nat. Mater., 2017, 16(9): 925-931.

[81] Danilovic N, Subbaraman R, Chang K C, Chang S H, Kang Y J J, Snyder J, Paulikas A P, Strmcnik D, Kim Y T, Myers D, Stamenkovic V R, Markovic N M. Activity-stability trends for the oxygen evolution reaction on monometallic oxides in acidic environments[J]. J. Phys. Chem. Lett., 2014, 5(14): 2474-2478.

[82] Ouimet R J, Glenn J R, De Porcellinis D, Motz A R, Carmo M, Ayers K E. The role of electrocatalysts in the development of gigawatt-scale PEM electrolyzers[J]. ACS Catal., 2022, 12(10): 6159-6171.

[83] Hubert M A, King L A, Jaramillo T F. Evaluating the case for reduced precious metal catalysts in proton exchange membrane electrolyzers[J]. ACS Energy Lett., 2022, 7(1): 17-23.

[84] Liu Y P, Liang X, Chen H, Gao R Q, Shi L, Yang L, Zou X X. Iridium-containing water-oxidation catalysts in acidic electrolyte[J]. Chin. J. Catal., 2021, 42(7): 1054-1077.

[85] Wan G, Freeland J W, Kloppenburg J, Petretto G, Nelson J N, Kuo D Y, Sun C J, Wen J G, Diulus J T, Herman G S, Dong Y Q, Kou R H, Sun J Y, Chen S, Shen K M, Schlom D G, Rignanese G M, Hautier G, Fong D D, Feng Z X, Zhou H, Suntivich J. Amorphization mechanism of $SrIrO_3$ electrocatalyst: How oxygen redox initiates ionic diffusion and structural reorganization[J]. Sci. Adv., 2021, 7(2): eabc7323.

[86] Yang L, Yu G T, Ai X, Yan W S, Duan H L, Chen W, Li X T, Wang T, Zhang C H, Huang X R, Chen J S, Zou X X. Efficient oxygen evolution electrocatalysis in acid by a perovskite with face-sharing IrO_6 octahedral dimers[J]. Nat. Commun., 2018, 9: 5236.

[87] Yang L, Zhang K X, Chen H, Shi L, Liang X, Wang X Y, Liu Y P, Feng Q, Liu M J, Zou X X. An ultrathin two-dimensional iridium-based perovskite oxide electrocatalyst with highly efficient {001} facets for acidic water oxidation[J]. J. Energy Chem., 2022, 66: 619-627.

[88] Gao R Q, Zhang Q, Chen H, Chu X F, Li G D, Zou X X. Efficient acidic oxygen evolution reaction electrocatalyzed by iridium-based 12L-perovskites comprising trinuclear face-shared IrO_6 octahedral strings[J]. J. Energy Chem., 2020, 47: 291-298.

[89] Geiger S, Kasian O, Ledendecker M, Pizzutilo E, Mingers A M, Fu W T, Diaz-Morales O, Li Z Z, Oellers T, Fruchter L, Ludwig A, Mayrhofer K J J, Koper M T M, Cherevko S. The stability number as a metric for electrocatalyst stability benchmarking[J]. Nat. Catal., 2018, 1(7): 508-515.

[90] Zhang Q, Chen H, Yang L, Liang X, Shi L, Feng Q, Zou Y C, Li G D, Zou X X. Non-catalytic, instant iridium (Ir) leaching: A non-negligible aspect in identifying Ir-based perovskite oxygen-evolving electrocatalysts[J]. Chin. J. Catal., 2022, 43(3): 885-893.

[91] Liang X, Shi L, Liu Y P, Chen H, Si R, Yan W S, Zhang Q, Li G D, Yang L, Zou X X. Activating inert, non-precious perovskites with iridium dopants for efficient oxygen evolution reaction under acidic conditions[J]. Angew. Chem. Int. Ed., 2019, 58(23): 7631-7635.

[92] Chen H, Shi L, Liang X, Wang L N, Asefa T, Zou X X. Optimization of active sites via crystal phase, composition, and morphology for efficient low-iridium oxygen evolution catalysts[J]. Angew. Chem. Int. Ed., 2020, 59(44): 19654-19658.

[93] Liang X, Shi L, Cao R, Wan G, Yan W S, Chen H, Liu Y P, Zou X X. Perovskite-type solid solution nano-electrocatalysts enable simultaneously enhanced activity and stability for oxygen evolution[J]. Adv. Mater., 2020, 32(34): 2001430.

[94] Shi L, Chen H, Liang X, Liu Y P, Zou X X. Theoretical insights into nonprecious oxygen-evolution active sites in Ti-Ir-Based perovskite solid solution electrocatalysts[J]. J. Mater. Chem. A, 2020, 8(1): 218-223.

[95] Feng W Q, Chen H, Zhang Q, Gao R Q, Zou X X. Lanthanide-regulated oxygen evolution activity of face-sharing IrO_6 dimers in 6H-perovskite electrocatalysts[J]. Chin. J. Catal., 2020, 41(11): 1692-1697.

[96] Zhang R H, Pearce P E, Pimenta V, Cabana J, Li H F, Dalla Corte D A, Abakumov A M, Rousse G, Giaume D, Deschamps M, Grimaud A. First example of protonation of ruddlesden-popper Sr_2IrO_4: A route to enhanced water oxidation catalysts[J]. Chem. Mater., 2020, 32(8): 3499-3509.

[97] Kim B J, Abbott D F, Cheng X, Fabbri E, Nachtegaal M, Bozza F, Castelli I E, Lebedev D, Schäublin R, Copéret C, Graule T, Marzari N, Schmidt T J. Unraveling thermodynamics, stability, and oxygen evolution activity of strontium ruthenium perovskite oxide[J]. ACS Catal., 2017, 7

(5): 3245-3256.

[98] Retuerto M, Pascual L, Calle-Vallejo F, Ferrer P, Gianolio D, Pereira A G, García Á, Torrero J, Fernández-Díaz M T, Bencok P, Peña M A, Fierro J L G, Rojas S. Na-doped ruthenium perovskite electrocatalysts with improved oxygen evolution activity and durability in acidic media[J]. Nat. Commun., 2019, 10: 2041.

[99] Hirai S, Ohno T, Uemura R, Maruyama T, Furunaka M, Fukunaga R, Chen W T, Suzuki H, Matsuda T, Yagi S. $Ca_{1-x}Sr_xRuO_3$ perovskite at the metal-insulator boundary as a highly active oxygen evolution catalyst[J]. J. Mater. Chem. A, 2019, 7(25): 15387-15394.

[100] Ji M W, Yang X, Chang S D, Chen W X, Wang J, He D S, Hu Y, Deng Q, Sun Y, Li B, Xi J Y, Yamada T, Zhang J T, Xiao H, Zhu C Z, Li J, Li Y D. RuO_2 clusters derived from bulk $SrRuO_3$: Robust catalyst for oxygen evolution reaction in acid[J]. Nano Res., 2022, 15(3): 1959-1965.

[101] Miao X B, Zhang L F, Wu L, Hu Z P, Shi L, Zhou S M. Quadruple perovskite ruthenate as a highly efficient catalyst for acidic water oxidation[J]. Nat. Commun., 2019, 10: 3809.

钙钛矿型水氧化电催化剂

梁 宵,张可新,沈雨澄,孙 轲,石 磊,陈 辉,郑克岩*,邹晓新*

(吉林大学化学学院,无机合成与制备化学国家重点实验室,吉林 长春 130012)

摘要: 在全球能源结构“清洁化”转型的背景下,可再生能源的开发与利用能够有效解决能源危机与环境问题,符合我国的可持续发展路线。能源转换与储存技术贯穿着循环能源技术的各个环节,是新型能源框架的核心支撑。水氧化反应是众多能源体系(例如,水裂解反应、二氧化碳还原反应、氮还原反应和金属-空气电池)的重要半反应,但其动力学缓慢,严重限制了设备的能源效率,阻碍了相应技术的广泛应用。因此,亟需开发具有低成本、高活性、强稳定性的水氧化电催化剂以降低反应能垒,进而推动能源转换与存储设备的工业化发展。钙钛矿型材料的晶体结构包容性强,元素组成涵盖广泛,具有丰富而独特的电子特性,易于实现表面化学与电子结构的精准调控,因此被公认为理想的催化材料设计平台。本文综述了钙钛矿型水氧化电催化剂的最新研究进展。首先介绍了钙钛矿型材料的晶体结构和电子特性,归纳了制备钙钛矿型氧化物的代表性的合成策略。通过讨论近期钙钛矿型水氧化电催化剂在酸性和碱性介质中的研究进展,强调了钙钛矿型电催化剂结构与催化性能间的构效关系。最后,我们总结了钙钛矿型水氧化电催化剂在实际应用中面临的挑战与机遇,提出了相应的建议与解决方案,期望能使读者更清晰地认识到该领域的未来发展方向。

关键词: 钙钛矿;水氧化;电催化;水裂解;氢能